Climate Dynamics (2020) 55:1105–1124
https://doi.org/10.1007/s00382-020-05316-0

Wintertime Arctic Oscillation and North Atlantic Oscillation and their impacts on the Northern Hemisphere climate in E3SM

Doo Young Lee[1] · **Wuyin Lin**[2] · **Mark R. Petersen**[1]

Received: 19 December 2019 / Accepted: 26 May 2020 / Published online: 1 June 2020
© Springer-Verlag GmbH Germany, part of Springer Nature 2020

Abstract

The characteristics of the wintertime Arctic Oscillation (AO) and North Atlantic Oscillation (NAO) and their impacts on climate variability over the Northern Hemisphere are important metrics for evaluating a climate system model. Observational analyses reveal that the horizontal and vertical structures in the AO and NAO exhibit a meridional dipole and a large-scale barotropic pattern between the Arctic and mid-latitudes. Historical model simulations from the Energy Exascale Earth System Model (E3SM-HIST) are used to identify how well it captures these major climate modes. It is found that the simulated AO and NAO modes have spatial structures similar to the observed features. In addition, the observed frequency bands in the AO and NAO-related time variability are captured well in the E3SM-HIST simulation. Associated with the positive phase in wintertime AO and NAO, zonal flow and warm advection in mid-latitude continents are enhanced, along with stronger cold flow from enhanced northerly winds over high latitudes. These features are linked to the atmospheric circulation pattern reflected by lower SLP anomalies over the Arctic and higher SLP anomalies over the mid-latitudes. In E3SM-HIST, these spatial associations and main structural features are analogous to those in observations. In the time-height evolution related to winter AO and NAO modes, it can also be seen that the simulations reproduce the downward propagating patterns in observations. Nevertheless, the vertical structures associated with AO and NAO in E3SM-HIST exhibit substantial biases in the lower stratosphere. The cause of these stratospheric biases is investigated using the strength of climatological stratospheric polar vortex (SPV) and wave activity fluxes. The results herein suggest that E3SM-HIST has a reasonable skill in reproducing the observed characteristics related to the winter AO and NAO, although there exist systematic biases in the associated climate variability.

Keywords Arctic Oscillation (AO) · North Atlantic Oscillation (NAO) · Energy Exascale Earth System Model (E3SM) · Wintertime climate variability modes · Winter AO and NAO-related climate impacts

1 Introduction

The Arctic Oscillation (AO) is defined as the leading mode of extra-tropical low-frequency variability and is characterized by a large-scale barotropic and zonally symmetric seesaw pattern of pressure anomalies between the Arctic and mid-latitudes of the Northern Hemisphere (Thompson and Wallace 1998, 2000, 2001; Zuo et al. 2013b; Gong et al. 2017). The AO is also referred to as the Northern Hemisphere annular mode (NAM). Many previous studies (Thompson and Wallace 1998, 2000, 2001; Gong et al. 2001; Wu and Wang 2002; Wang and Chen 2010; Chen et al. 2013; He et al. 2017) have demonstrated that different phases of the AO can control the meridional temperature gradient by the air mass change and have important impacts on climate variability over wide regions of the Northern Hemisphere.

The North Atlantic Oscillation (NAO) is the most dominant pattern of atmospheric variability and plays an important role in climate variations over regions between eastern North America and the Eurasian continent, especially during the cold season (van Loon and Rogers 1978; Wallace and Gutzler 1981; Hurrell 1995, 1996; Kushnir 1999; Greatbatch 2000; Marshall et al. 2001; Hurrellet al. 2003; Hurrell and Deser 2015). The positive phase of the NAO is characterized

✉ Doo Young Lee
dylee@lanl.gov; dylee1220@gmail.com

[1] Computational Physics and Methods (CCS-2), Los Alamos National Laboratory, P.O. Box 1663, Los Alamos, NM 87545, USA

[2] Environmental and Climate Sciences Department, Brookhaven National Laboratory, Upton, NY, USA

by stronger westerly winds and warm temperature anomalies over the North Atlantic Ocean and Eurasian continent along with weaker westerlies and cold temperature anomalies over the eastern Canadian Arctic and western Greenland.

The AO and NAO are both important modes of wintertime climate variability in the Northern Hemisphere. The AO pattern has remarkable similarities to the NAO, with the largest signal over the Atlantic sector. Their indices are highly correlated, but the AO pattern is zonally more symmetric with one center of action over the Arctic region and an annular structure with opposite sign at mid-latitudes. AO and NAO also describe similar climate phenomena, but lead to different dynamical interpretations (Deser 2000; Greatbatch 2000; Wallace 2000; Ambaum et al. 2001; Wanner et al. 2001). The signals of both AO and NAO are not confined to the surface. They also reach up to the middle atmosphere (Wallace and Gutzler 1981; Kushnir and Wallace 1989; Thompson and Wallace 2000; Wanner et al. 2001; Zuo et al. 2013b).

The ability of coupled global climate models (CGCMs) to simulate the AO and NAO variability is an important indicator of model performance. The simulated AO and NAO patterns have been widely evaluated using the climate models taking part in the Coupled Model Intercomparison Project Phase 3 (CMIP3) and phase 5 (CMIP5) (Miller et al. 2006; Xin et al. 2008; Stoner et al.2009; Zhu and Wang 2010; Driscoll et al. 2012; Cattiaux and Cassou 2013; Zuo et al. 2013b; Davini and Cagnazzo 2014; Gong et al. 2017). It has been demonstrated that almost all the models are able to reproduce the horizontal and vertical patterns of the AO and NAO, whereas their ability to simulate the magnitude and location of the patterns as well as their temporal variability needs to be improved as compared to observations (Zuo et al. 2013b; Gong et al. 2017, 2019a).

We analyze the characteristics of the wintertime AO and NAO, and investigate their impacts on climate variability over the Northern Hemisphere to identify how well the major climate variability modes are captured in the Energy Exascale Earth System Model (E3SM) as a coupled climate system. We use the E3SM historical simulations (E3SM-HIST) with five ensemble members and several reanalysis products over the period of 36 years since the satellite era to evaluate the performance of the variability and influence of the AO and NAO climate modes. The primary goal of this study is to contribute to the improvement of the E3SM simulation through an analysis of the model results, and document and understand the current status and deficiency of the model in simulating the AO and NAO patterns.

A description of the model, the simulated and reanalysis datasets, and the methods employed in this study is provided in Sect. 2. In Sect. 3, we describe the observed vertical variability and seasonality related to observed monthly AO and NAO modes. Section 4 presents the wintertime AO and NAO-associated horizontal and vertical structures and Sect. 5 analyzes the characteristics of AO and NAO winter indices. The wintertime AO and NAO-associated climate impacts are provided in Sect. 6. A possible cause of stratospheric biases is discussed in Sect. 7. Finally, a summary and conclusions are presented in Sect. 8.

2 Model, data and methodology

2.1 Energy Exascale Earth System Model version 1 (E3SM)

E3SM is a new global climate coupled model funded by the U.S. Department of Energy (DOE) and includes five component models. The low-resolution configuration of the E3SM is used in this study. The atmospheric component is E3SM Atmosphere Model (EAM) with a spectral element dynamical core at 110-km resolution on a cubed sphere geometry and 72 layers with a top at approximately 60 km (Rasch et al. 2019; Tang et al. 2019). The oceanic component is the Model for Prediction Across Scales-Ocean (MPAS-Ocean), which runs on an unstructured C-grid (Arakawa and Lamb 1977) of near-hexagons, varying from 30 to 60 km in the horizontal direction with 60 vertical layers (Ringler et al. 2010; Petersen et al. 2015, 2019). The sea ice component is the MPAS-Seaice. MPAS-Seaice and MPAS-Ocean share identical meshes, but MPAS-Seaice uses a B-grid (Arakawa and Lamb 1977) with sea ice concentration, volume, and tracers defined at cell centers and velocity defined at cell vertices (Hunke and Dukowicz 1997; Petersen et al. 2019). The E3SM Land Model version 0 (ELMv0), which is the land component in E3SM version 1 (Golaz et al. 2019), describes interactions of the land surface with the near-surface atmosphere and includes interactions among land subsystems such as vegetation, soil, snow, groundwater, runoff, urban areas, and managed ecosystems (Oleson et al 2013). The river transport model in E3SM use the Model for Scale Adaptive River Transport (MOSART) for a more physically based representation of riverine processes (Li et al. 2013, 2015). E3SM is the first climate system model that is capable of regional refinement of the horizontal grid for all components. The model uses unstructured-mesh arrays where neighbors are defined by pointer variables, rather than structured meshes on regular latitude/longitude grids. More detailed descriptions of the E3SM fully coupled model can be found in Golaz et al. (2019).

2.2 Data

We use the historical simulation (hereafter E3SM-HIST) dataset, which contributes to the Coupled Model Intercomparison Project Phase 6 (CMIP6: Eyring et al. 2016).

Historical simulations covering the period 1850 through the end of 2014 are forced by external factors such as natural (e.g., solar variability, volcanic aerosols) and anthropogenic (e.g., CO_2 concentration, aerosols, and land use) forcing based on time-dependent observations. For this study, we use various surface and three-dimensional variables for the 36-year period of 1979–2014 in E3SM-HIST, which has five ensemble members. The same variables and time period as for the model simulations are used for the corresponding observed datasets. In order to compare to observed gridded data, we perform horizontal interpolation using a mapping file to re-grid all unstructured variables of E3SM-HISTsimulation onto a 256 × 129 (about 1.4° × 1.4°) longitude-latitude grid. The target season is boreal winter, January through March (JFM) for 36 years. To assess the performance of the E3SM-HIST simulation, several observational data are used: Fifth generation of European Centre for Medium-Range Weather Forecasts (ECMWF) atmospheric reanalysis of the global climate (ERA5: Hersbach et al. 2018), National Centers for Environmental Prediction (NCEP)-Department of Energy (DOE) reanalysis 2 (NCEP-R2: Kanamitsu et al. 2002), Global Precipitation Climatology Project Version 2.3 Combined Precipitation Dataset (GPCP: Adler et al. 2003), Climate Prediction Center (CPC) Merged Analysis of Precipitation (CMAP: Xie and Arkin 1997), and Hadley Centre Global Sea Ice and Sea Surface Temperature (HadISST: Rayner et al. 2003). All observed datasets are interpolated onto the same horizontal grid as simulation. The datasets used in this study are summarized in Table 1.

2.3 Methods

AO and NAO modes are defined as the first empirical orthogonal function (EOF) of the winter-time mean SLP anomalies in the circumpolar region of 20–90° N (Thompson and Wallace 2000; Hurrell and Deser 2015) and in the North Atlantic sector, 20–80° N, 90° W–40° E (Hurrell et al. 2003; Hurrell and Deser 2010), respectively. The AO and NAO indices are the corresponding standardized principal component (PC1) time series, which are the amplitudes associated with the first eigenvector based on the covariance matrix. These PCs are standardized by subtracting the mean and dividing by the standard deviation, respectively. The regression coefficients of the SLP anomalies on the AO and NAO indices are defined as the AO and NAO patterns. For the E3SM-HIST simulations possessing five ensemble members, we take an equal-weight average of all members' corresponding AO (or NAO) patterns after obtaining the AO (or NAO) mode and time series by applying the same EOF analysis to each ensemble member. The averaged t value among each member was used to evaluate the confidence level of the ensemble mean pattern based on a two-tailed Student's t test (Gong et al. 2014, 2015, 2017, 2019a).

3 Variability and seasonality related to observed monthly AO and NAO

To find the vertical variability of climatic variables associated with observed monthly AO and NAO modes over the Northern Hemisphere, the zonal-mean vertical structures regressed onto the monthly AO and NAO indices based on monthly mean data from two reanalyses (ERA5 and NCEP-R2) are computed in Fig. 1. From the vertical structures, we can obtain the AO and NAO-associated vertical variability and their features corresponding to the polarities of both climate modes. Figure 1 shows the vertical regression fields of the geopotential height (Z), zonal wind (U), and temperature (T) anomalies observed in association with the monthly AO and NAO indices. These structures are similar to the results of Greatbatch (2000), Thompson and Wallace (2000), and Zuo et al. (2013b). These regression patterns, based on the AO and NAO indices, are very similar to each other and exhibit a distinct signature in

Table 1 Reanalysis and simulated datasets used

Name	Observational (reanalysis) data				Simulated data
	ERA5	NCEP-R2	GPCP/CMAP	HadISST	E3SMv1 (Energy Exascale Earth System Model version 1)
Variable	Sea Level Pressure (SLP)		Precipitation (PREC)	Sea Surface Temperature (SST)	
	Geopotential Height (Z)				E3SM-HIST (Historical simulation)
	Zonal wind (U)				5 ensemble members
	Temperature (T)				SLP, Z, U, T, PREC, and SST
Resolution	1440 × 721 (0.25° × 0.25°)	144 × 73 (2.5° × 2.5°)	144 × 72 (2.5° × 2.5°)	360 × 180 (1° × 1°)	256 × 129 (1.4° × 1.4°)

Target season: January–March (JFM, Boreal winter)

Period: 1979–2014 (36 years)

Vertical variables (Z, U, and T) use the 17 vertical pressure levels of 1000–10 hPa

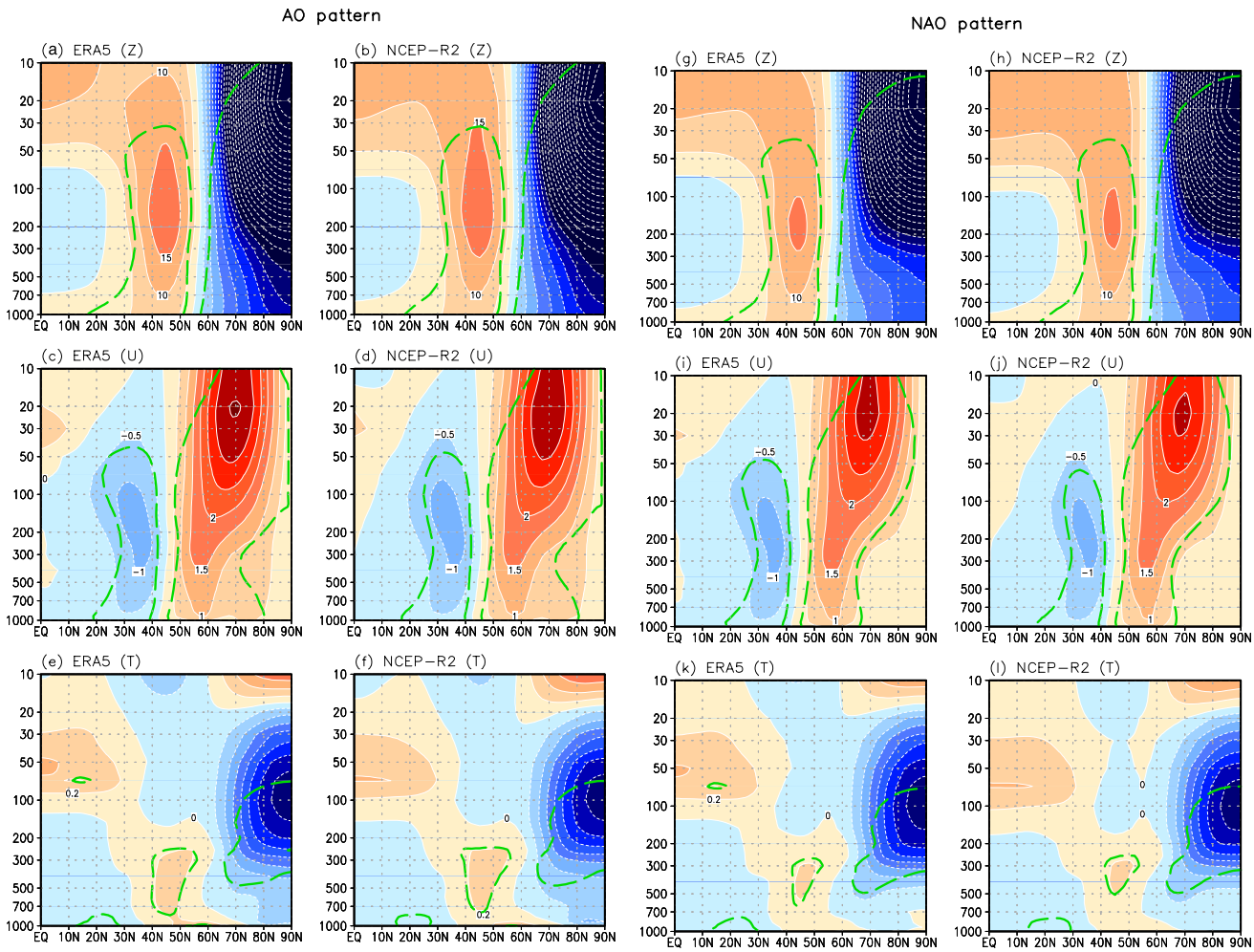

Fig. 1 Vertical structures of the zonal-mean (top) geopotential height (Z, unit: m), (middle) zonal wind (U, unit: m/s), and (bottom) temperature (T, unit: K) regressed on the observed monthly **a–f** AO and **g–l** NAO indices based on monthly mean data from Jan 1979 to Dec 2014 for ERA5 and NCEP-R2. Contour intervals are 5 m for geopotential height, 0.5 m/s for zonal wind, and 0.2 K for temperature. Green dashed line indicates statistical significance at the 95% confidence level for a two-tailed Student's *t* test

the geopotential height and zonal wind fields, indicated by a zonally symmetric and equivalent barotropic structure from the surface to the lower stratosphere. AO and NAO modes have dominant dipole meridional structures with nodes of opposite signs separated near 55° N for geopotential height and near 45° N for zonal wind. The largest geopotential height anomalies in the AO and NAO modes are observed in the lower stratosphere near 20 hPa. The high-latitude centers of zonal wind have maxima centered near 60° N in the lower troposphere and about 70° N in the lower stratosphere (20 hPa). The poleward tilting with height in the regressed zonal wind fields shows maximum wind activity of the AO and NAO modes amplified with height upward into the lower stratosphere. The positive monthly AO and NAO modes are marked by anomalously cold polar cap regions, with the largest negative anomalous temperature in the tropopause near 100 hPa.

Based on the vertical location of the largest variability for the geopotential height, zonal wind and temperature related to the monthly observed AO and NAO modes, the annual variations calculated from monthly anomalies are obtained following the method of Thompson and Wallace (2000) (Fig. 2). Monthly mean 20 hPa geopotential height (Z20) and zonal wind (U20), 100 hPa temperature (T100), and sea level pressure (SLP) anomalies are averaged over the region poleward of 70° N for the 36-year period 1979–2014, and their annual cycles are repeated in the display. In addition, the magnitude of annual variation is calculated for each month and variable (Table 2). We can find that the magnitudes of the amplitudes are somewhat larger during the cold season (December–April) and the structures shown in Fig. 1 are largely dominated by the cold season. The upper-level anomalies (Z20, U20, and T100) averaged over the polar cap regions exhibit much stronger seasonality than that of

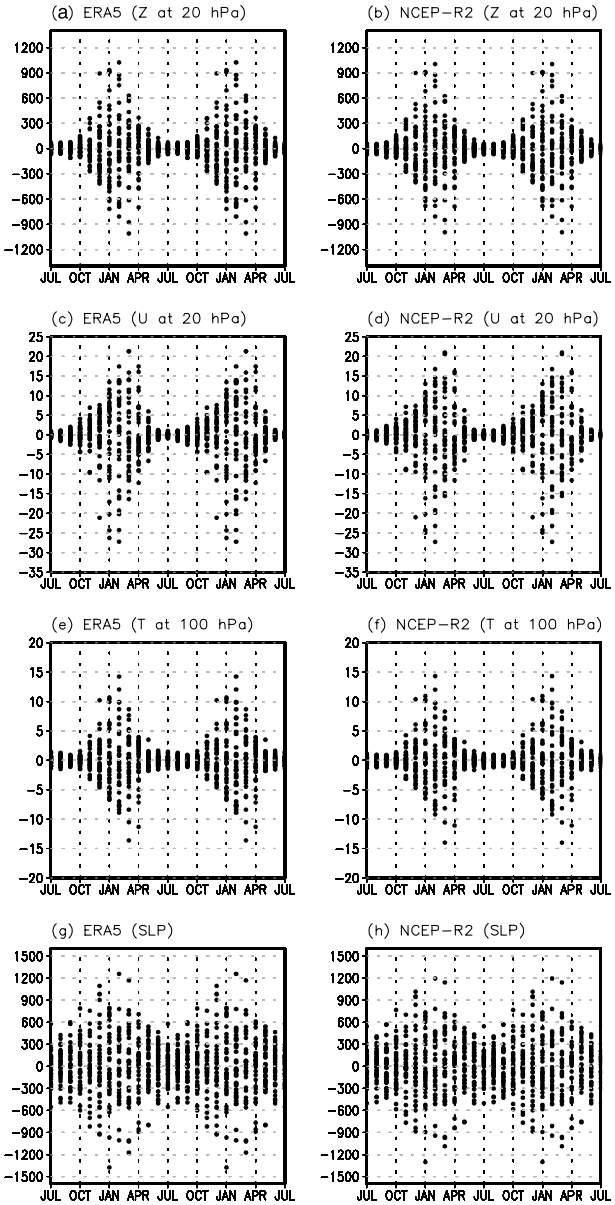

Fig. 2 Annual variation of observed monthly mean anomalies for **a**, **b** geopotential height (unit: m) at 20 hPa, **c**, **d** zonal wind (unit: m/s) at 20 hPa, **e**–**f** temperature (unit: K) at 100 hPa, and **g**, **h** sea level pressure (unit: hPa) averaged over the region poleward of 70° N for the 36 years (1979–2014). Annual variance is depicted together repeatedly

the low-level anomalies (SLP). The distribution of monthly SLP anomalies also shows higher amplitudes during the cold season, but it is not as clear as the upper-level variables due to the higher variance during the warm season. The distribution of Z20 anomalies is slightly skewed to early or later months of the cold season for positive and negative anomalies, respectively. This shape is similar to the distribution of T100 anomalies, but the pattern of U20 anomalies is skewed in the opposite direction. Overall from these results, it can

Table 2 Magnitude of annual variation for each month and variable

	Magnitude of variation (Max–Min)												
	Jan	Feb	Mar	Apr	May	Jun	Jul	Aug	Sep	Oct	Nov	Dec
ERA5 (Z20, unit: m)	1653.62	1833.01	1639.94	1067.96	404.812	218.761	137.768	129.259	187.5	250.304	631.315	1310.1
NCEP-R2 (Z20, unit: m)	1593.17	1812.56	1618.22	1030.65	367.598	197.793	127.302	119.649	174.495	270.685	623.142	1301.88
ERA5 (U20, unit: m/s)	39.7371	44.6893	37.7049	29.7186	12.5946	2.4519	1.90263	2.6537	4.52723	8.46751	16.5627	28.7165
NCEP-R2 (U20, unit: m/s)	37.9706	44.0548	36.5486	27.7229	12.7923	2.5842	2.14488	2.46903	4.48215	8.48862	16.111	28.4095
ERA5 (T100, unit: K)	17.3707	23.1474	22.2941	15.2689	5.29947	3.16752	2.87352	2.78132	2.04999	3.04249	7.38062	14.8063
NCEP-R2 (T100, unit: K)	17.377	23.4883	22.2867	14.6927	4.63714	3.21061	2.41219	2.10698	1.91749	2.62193	7.42533	15.0712
ERA5 (SLP, unit: hPa)	2170.81	2263.75	2339.29	1598.49	1342.45	969.301	1130.9	913.85	1088.12	1385.92	1573.87	2020.4
NCEP-R2 (SLP, unit: hPa)	2034.74	2137.05	2228.89	1535.53	1283.62	934.118	1046.23	891.915	993.963	1349.65	1470.26	1899.37

be clearly seen that the AO and NAO modes are most active during January–February–March (JFM) (Thompson and Wallace 2000), so we consider JFM to be the boreal winter season in this study.

4 Horizontal and vertical structures related to wintertime AO and NAO

In the previous section we showed that climate variables related to AO and NAO modes have larger variability during the JFM winter season. Here we focus on comparing the JFM mean sea level pressure (SLP) anomaly patterns regressed on the JFM AO and NAO indices for two reanalyses and E3SM-HIST simulation in Fig. 3. The observed structures related to the AO mode, which explains 31.9% (ERA5) and 31.8% (NCEP-R2) of the total variance, show a zonally symmetric pattern, which is characterized by north–south seesaws of atmospheric mass between the Arctic region and the mid-latitudes. These features are consistent with previous studies (Thompson and Wallace 1998, 2000; Miller et al. 2006; Zuo et al. 2013b; Hurrell and Deser 2015; Gong et al. 2017). The spatial pattern correlation coefficient (PCC) of AO-related SLP patterns between ERA5 and NCEP-R2 dataset is 0.997 over the Northern Hemisphere. The observed NAO-related SLP anomaly patterns, which have the explained variance of 50.1% for ERA5 and 50.0% for NCEP-R2, exhibit similar amplitudes and meridional scales compared to the observed AO SLP anomaly patterns, although there are some differences that show slightly reduced and increased amplitudes over the North Pacific and Atlantic Ocean, respectively. Previous studies (Rogers and McHugh 2002; Feldstein and Franzke 2006; Gong et al. 2017) also mentioned that the wintertime AO and NAO are somewhat difficult to distinguish in observations. The E3SM-HIST simulation reproduces the AO and NAO-related SLP anomaly patterns quite well. The PCCs of the E3SM-HIST simulation with observations have comparable values higher than about 0.8. However, the E3SM-HIST tends to simulate an excessively strong (weak) Pacific and northern Europe (Atlantic) center of SLP anomaly patterns associated with AO and NAO modes. This feature can be seen in most of the climate models (Miller et al. 2006; Cattiaux and Cassou 2013; Gong et al. 2017). Note that Gong et al. (2018, 2019b) found the pattern of the AO over the North Pacific center varies with time in observations. The excessively strong North Pacific center in E3SM, however, is not due to such temporal variation. The amplitude and size of the AO patterns over the North Pacific in E3SM-HIST simulations consistently showed the same biases when the analysis was performed over different periods of time (figure not shown). Gong et al. (2017) considered a statistical method for bias-correction to improve the pattern and teleconnections of AO in the CMIP5 models. From the same bias-corrected AO pattern in E3SM-HIST simulation

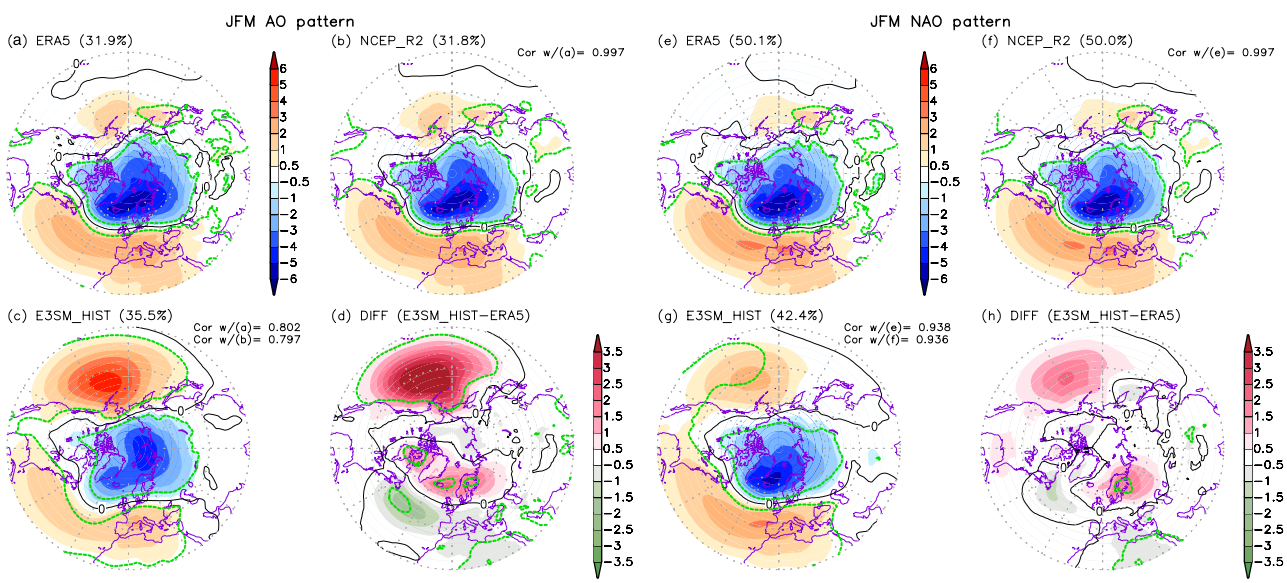

Fig. 3 Wintertime (January-March: JFM) mean sea level pressure (SLP, unit: hPa) anomaly patterns regressed on the JFM **a–c** AO and **e–g** NAO indices over the Northern Hemisphere (20–90° N) in **a**, **e** ERA5, **b**, **f** NCEP-R2, and **c**, **g** E3SM-HIST dataset for the period 1979–2014. **d**, **h** The difference patterns between E3SM-HIST and ERA5. Percentages indicate explained variance (averaged explained variance from each ensemble member for E3SM-HIST) from the pattern. Green dashed line indicates statistical significance at the 95% confidence level for a two-tailed Student's *t* test

(not shown), the method was also found to be useful for improvement of the AO-related variability although it is not used in this study.

In Fig. 4, similar to monthly AO and NAO-associated vertical structures in Fig. 1, the wintertime zonally-averaged vertical regressed structures are investigated in terms of JFM AO and NAO modes in observations and E3SM-HIST simulation. The patterns of observed wintertime regression fields are remarkably similar to those of the corresponding monthly fields for each variable in Fig. 1, while some differences in the amplitude are shown. The simulated vertical structures associated with JFM AO and NAO modes for geopotential height and zonal wind in E3SM-HIST display to some extent the similar patterns as observed. The E3SM-HIST is able to reproduce the observed negative barotropic geopotential height anomalies (Fig. 4c, l) and the observed westerly anomalies tilting poleward with height (Fig. 4f, o) in the high-latitudes. But it shows difficulties in simulating the variability for the two variables in the mid and high latitudes of the stratosphere. For example, the E3SM simulation displays the maximum center of the AO and NAO-associated vertical structure at lower altitudes (biased downward to the troposphere or tropopause) compared to the observations. In addition, the amplitudes of the simulated vertical structures associated with the AO and NAO modes, especially in the high latitude, are much weaker than those of observed. Figure 5 exhibits the vertical relationship between two observations and E3SM-HIST for JFM AO and NAO-associated zonally-averaged vertical structures. As mentioned above, due to the significant stratospheric biases in both magnitude and location of vertical patterns for geopotential height and zonal wind, the skill is low in capturing the characteristics of the observations in the stratosphere (see also Zuo et al. 2013b), while we can find a high correlation between observed and simulated vertical patterns associated with winter AO and NAO modes in the troposphere or even up to the lower portion of the lower stratosphere (Fig. 5a–d). In both AO and NAO-associated observed temperature (T), the spatial patterns are characterized by a deep layer of anomalously cold polar cap regions and an anomalously warm area centered about 45–50° N at surface. We can also see that the distribution of the observed positive temperature anomalies extends upward from the mid-latitude troposphere and forks into equatorward (to the tropical tropopause) and poleward (to the polar stratosphere)

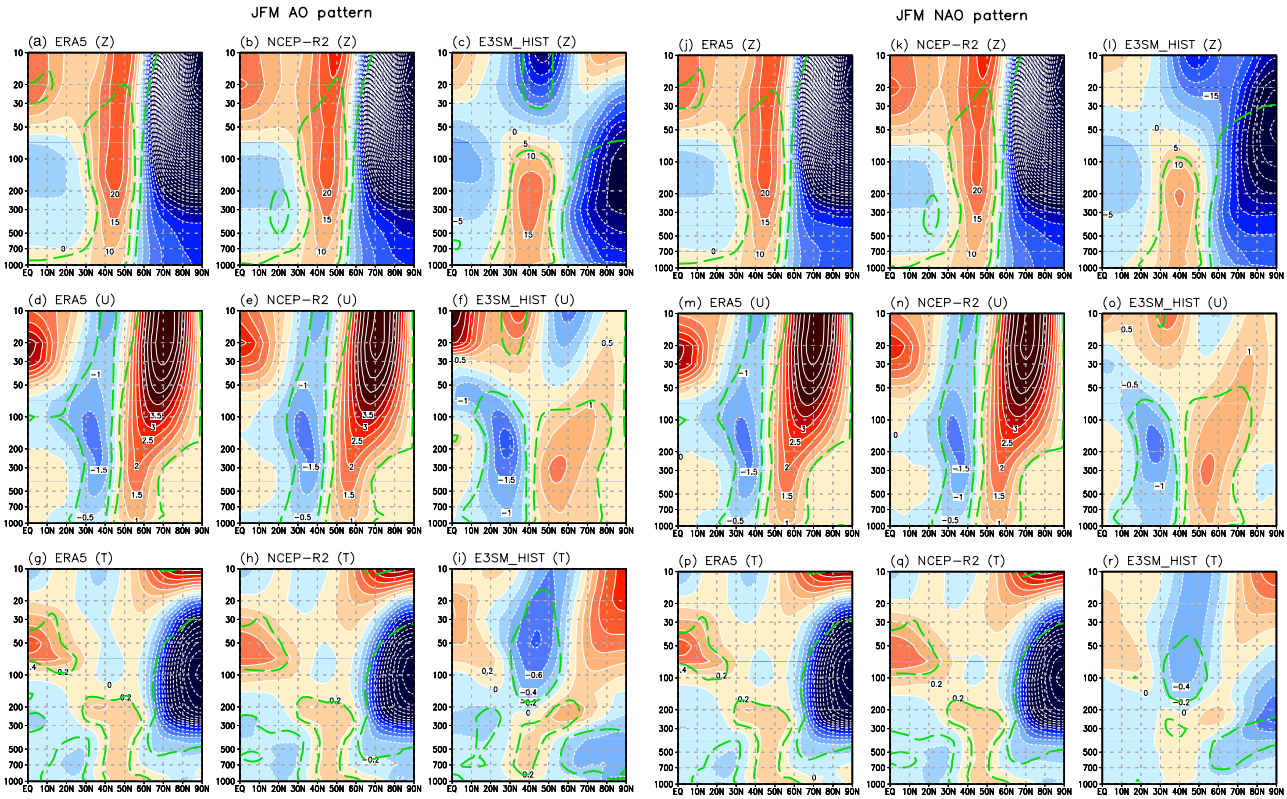

Fig. 4 Vertical structures of the wintertime (JFM) zonal-mean (top) geopotential height (Z, unit: m), (middle) zonal wind (U, unit: m/s), and (bottom) temperature (T, unit: K) regressed on the JFM **a–i** AO and **j–r** NAO indices in ERA5, NCEP-R2, and E3SM-HIST for the period 1979–2014. Contour intervals are 5 m for geopotential height, 0.5 m/s for zonal wind, and 0.2 K for temperature. Green dashed line indicates statistical significance at the 95% confidence level for a two-tailed Student's *t* test

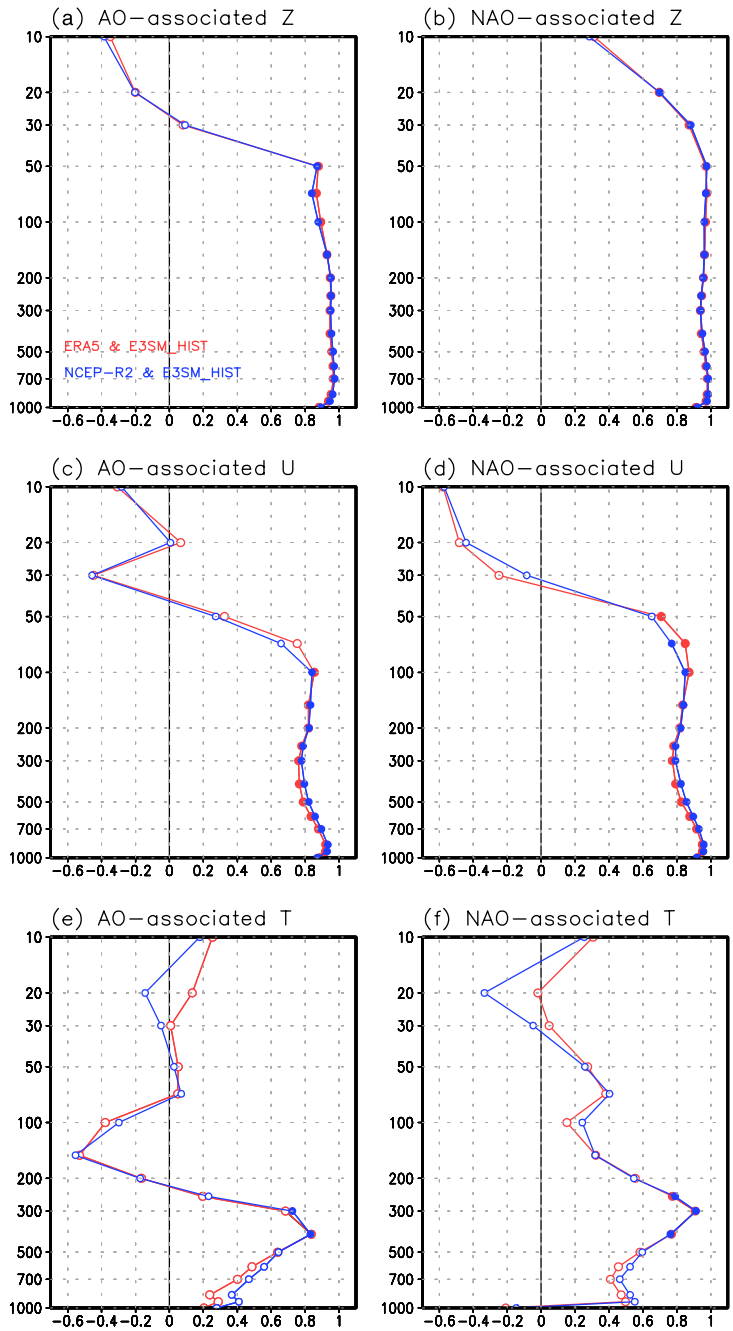

Fig. 5 Pattern correlation of the wintertime (JFM) zonally-averaged vertical structures for **a**, **b** geopotential height (Z), **c**, **d** zonal wind (U), and **e**, **f** temperature (T) associated with the JFM AO and NAO modes. Red (Blue) lines indicate spatial pattern correlation coefficients between ERA5 (NCEP-R2) and E3SM-HIST. Closed circles indicate statistical significance at the 90% confidence level for a two-tailed Student's *t* test

branches going further up from upper troposphere near 200 hPa. Note that the vertical structure of the distribution extending to the pole for observed temperature is different from that in Thompson and Wallace (2000). In the simulated vertical temperature structure associated with the AO and NAO modes, there is difficulty in reproducing the observed features due to a much weaker cold polar cap as well as strong stratospheric cold anomalies in the 30–50° N belt. From these results, it can be seen that JFM AO and NAO-associated simulated temperature anomalies have a weak relationship with observations at most altitudes, except for the middle-troposphere (Fig. 5e, f). Generally, wintertime NAO-associated vertical structures show slightly better performance compared to wintertime AO-associated vertical structures. Although it is limited to upper troposphere or tropopause, simulated geopotential height and zonal wind in E3SM-HIST describe reasonably well the observed vertical characteristics. However, the

simulated temperature shows more difficulty in capturing them.

5 Spectral analysis of winter AO and NAO indices

We have performed the power spectrum analysis to determine how the dominant modes of climate variability vary in time and to quantify the significant periodic oscillations in the time series of the wintertime AO and NAO indices (Wanner et al. 2001; Hurrell et al. 2003; Jevrejeva et al. 2003, 2005). By decomposing the wintertime AO and NAO indices in time-period space for ERA5 and NCEP-R2 reanalyses and E3SM-HIST simulation, a wavelet power spectrum is shown in Fig. 6a–c for AO and in Fig. 6g–i for NAO. In addition, the 3-year smoothed power spectrum in frequency-variance pattern is examined to test the spectral behavior of the JFM AO (Fig. 6d–f) and NAO (Fig. 6j–l) indices. In general, the spectrum patterns of the observed AO and NAO winter indices consist of the similar leading signals with near-identical periodicity, namely, 2.4–2.6, 3.5, 5–5.5 and 33-years. The observed winter wavelet spectra for the JFM AO index clearly reveal the significant power peaks at about 3–4-years between about 1986 and 1992 (Fig. 6a, b). It also represents the enhanced power at the lowest frequency (period of about 33-years) band, which is consistent with the NAO-related observed wavelet spectra. The observed wavelet power spectra for the NAO index exhibit similar power band to those for the AO index, but the power variances of wavelet spectra of AO index are on average larger. The wavelet spectra for the JFM AO index in E3SM-HIST are considerably analogous to those of the simulated JFM NAO index, except for the bands of about 2.5–3-years during 2006-2014 and about 3–5-years during 1992–2002. In the AO and NAO winter indices, both observed power spectra have the power variance increasing with period, while the power variance of E3SM-HIST simulation shows a reversed pattern. The spectral analysis for the simulated AO winter index shows that E3SM-HIST simulation captures well the mode near the 3.5-year cycle, but failed to capture the period of about 2.4–2.6 and 33-years. In the NAO-related power spectral analysis, the E3SM-HIST simulation shows skill in capturing the cycles of about 2.4 and 5–5.5-years, but has difficulty to capture the frequency bands around 3.5 and 33-years.

6 Climate impacts of winter AO and NAO

Many studies (Thompson and Wallace 1998, 2000; Marshall et al. 2001; Hurrell and van Loon 1997; Wanner et al. 2001; Hurrell and Deser 2015; He et al. 2017; Gong et al. 2017) showed that AO and NAO have major impacts on various wintertime climate patterns of the Northern Hemisphere. In this section, by regression of the hemispheric climate variables on the JFM AO and NAO indices, we investigate the influence on the atmospheric fields over the Northern Hemisphere due to the AO and NAO modes.

Figure 7 indicates that change in temperature at 2 m (T2m) and 950 hPa wind pattern are significantly correlated with variability of the JFM AO and NAO indices, especially over the wide regions between North America and Eurasia including the Arctic. The AO-associated observed winter temperatures over much of North America and from Europe to Asia show the anomalous warming due to the warm southeasterly wind from the subtropical Atlantic Ocean and enhanced westerly wind across the North Atlantic, while observed temperatures over Greenland, northeastern Canada and the northern oceans depict the anomalous cooling due to the cold air from stronger northerly flows (Fig. 7a, b). This pattern is strongly related to variabilities in the atmospheric circulation, which are reflected by negative SLP anomalies over the high latitudes of the North Atlantic and much of the Arctic, and pattern of positive SLP anomalies over the subtropical Atlantic (Fig. 3a, b). These features associated with AO mode are considerably similar to those of the NAO-associated observed winter temperatures and winds (Fig. 7e, f), even though there exist some differences in temperature by the slightly stronger wind patterns around the polar cap region compared to NAO mode. Many previous studies (Deser 2000; Ambaum et al. 2001; Wallace and Thompson 2002) also mentioned it is very difficult to distinguish the relative effects of AO and NAO. The AO and NAO-associated temperature and wind patterns from the E3SM-HIST simulation are consistent with those from two observations. However, in both AO and NAO modes, one can see significant cold biases over northern Europe and Siberia and strong warm biases over northeastern Canada, Greenland and southern Asia (Fig. 7d, h). Specifically, as mentioned in Sect. 4, it is shown that the AO-related anomalously cold temperature biases by enhanced northerly wind over Alaska due to the strong clock-wise flow over North Pacific need to be improved in E3SM simulations, just like most of the CMIP5 models analyzed in Gong et al. (2017), while the NAO-related cold temperature over northwestern North America due to weak North Pacific winds is similar to the observations. The PCCs (0.872 and 0.869) of the NAO-associated simulated temperature are higher than those (0.795 and 0.804) of the AO-associated temperature because of smaller biases over the North Pacific compared to the AO mode.

The dominant patterns of wintertime SST anomaly variability associated with JFM AO and NAO modes in North Atlantic Ocean are exhibited in Fig. 8. The AO and NAO-associated enhanced tripole-like SST anomalies spreading

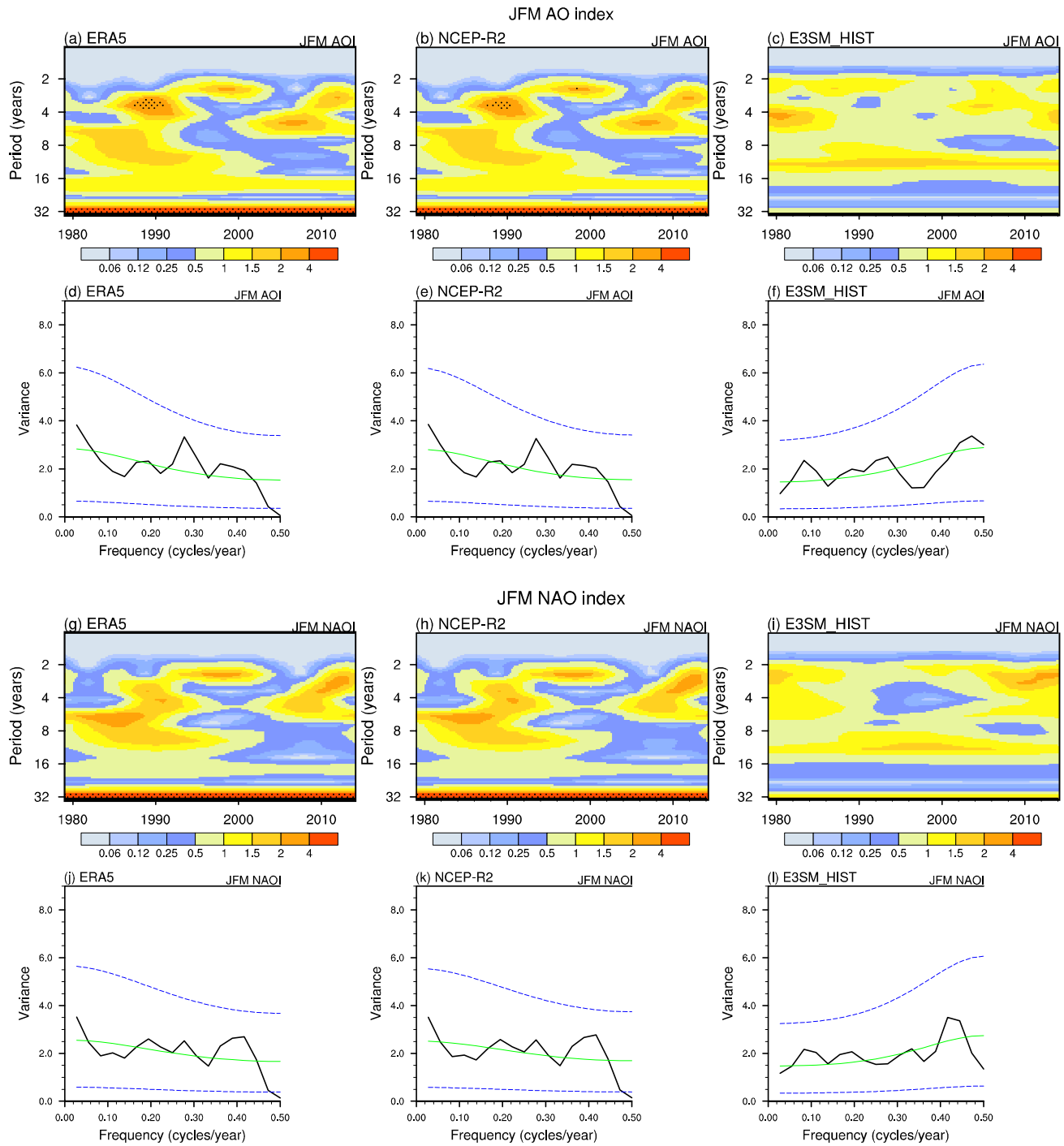

Fig. 6 **a–c** Wavelet power spectrum and **d–f** 3-year smoothed power spectrum (solid black) of the AO winter (JFM) index for (left) ERA5, (middle) NCEP-R2 and (right) E3SM-HIST during 1979–2014. Stippled areas at wavelet power spectrum indicate statistical significance at the 95% confidence level for a two-tailed Student's *t* test. Green solid and blue dashed lines at the power spectra show the red noise curve and the 95% confidence interval, respectively. **g–l** The same as **a–f** but for NAO winter (JFM) index

northeastward in observations (Fig. 8a, b) are consistent with the anomalous 2 m air temperature patterns over North Atlantic Ocean due to the subtropical Atlantic atmospheric circulation (Fig. 7a, e). This SST pattern is called the North Atlantic SST tripole pattern, which consists of a cold subpolar region, warm mid-latitudes and a cold region between

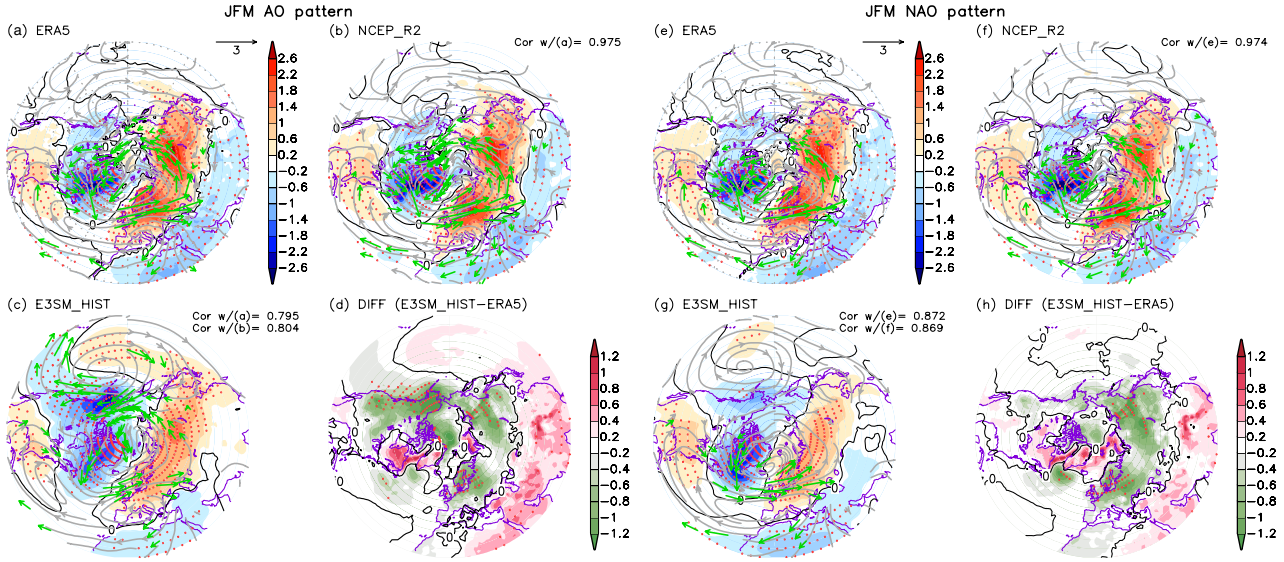

Fig. 7 Wintertime (JFM) 2 m temperature (T2m, unit: K), 925 hPa streamlines (gray contour, unit: m/s) and vector wind (green, unit: m/s) anomaly patterns regressed on the JFM **a**–**c** AO and **e**–**g** NAO indices over the Northern Hemisphere (20–90° N) in **a**, **e** ERA5, **b**, **f** NCEP-R2, and **c**, **g** E3SM-HIST dataset for the period 1979–2014. **d**, **h** The difference patterns between E3SM-HIST and ERA5. Red stippled area and green wind vector indicate statistical significance at the 95% confidence level for a two-tailed Student's *t* test

the equator and 30° N. Such tripole pattern typically occurs during the positive phase of AO and NAO over the North Atlantic Ocean (Czaja and Frankignoul 2002; Cohen and Barlow 2005; Zuo et al. 2013a). The AO and NAO-associated SST patterns from the E3SM-HIST simulation are similar to the observed SST patterns (Fig. 8c, d), but there exist significantly strong cold biases over the northwestern North Atlantic (Fig. 8e, f). In both the simulated and observed SST patterns, the North Atlantic tripole patterns appear to be more strongly affected by the NAO mode than the AO mode because the significant areas are much more widely distributed. The simulated SST tripole pattern associated with the NAO mode (PCC is 0.424), compare to AO mode (PCC is 0.302), show closer relationship with observed SST tripole pattern.

In Fig. 9, the distinct features in observed precipitation anomalies associated with AO and NAO winter modes are shown as a dipole mode over the Euro-Atlantic area. There are anomalously wet patterns, due to the northeastward shifts of relatively warm and moist maritime air (in Fig. 7), over the northern North Atlantic, which extends eastward across the northern Europe and Scandinavia, while anomalously dry conditions are present in the mid-latitude North Atlantic, much of southern Europe and northern portions of the Mediterranean. Changes in the intensity and pattern of climate variables, such as temperature, pressure, and precipitation fields, are caused by the changes in atmospheric circulation over the North Atlantic associated with the AO and NAO (Hurrell and van Loon 1997; Thompson and Wallace 2001; Hurrell and Deser 2015). This study also proves that the changes in wind circulation over the Atlantic in Fig. 7 is closely linked to large-scale anomaly patterns in precipitation (Fig. 9) as well as temperature (Fig. 7) in the same location. The simulated precipitation anomalies during the positive AO and NAO winters (Fig. 9c, g) show a considerable similarity to the observations both in their spatial pattern and magnitude over the Euro-Atlantic area. However, the strong dry and wet biases of the AO-associated precipitation anomaly in simulations over the eastern and western North Pacific still remain a challenge to be resolved (Fig. 9d), while the simulated NAO-associated precipitation anomaly shows weaker dry and wet biases in the North Pacific compared to the simulated AO-associated precipitation pattern.

In both the model and observations, the spatial patterns and biases of 500 hPa geopotential height (Z500) anomalies associated with AO and NAO modes (Fig. 10) are almost the same as those of SLP anomalies in Fig. 3. This reflects the quasi-barotropic characteristics of the vertical structure of the AO and NAO modes (Thompson and Wallace 2000; Greatbatch 2000; Zuo et al. 2013b; Gong et al. 2017). The observed patterns maintain these features through the lower stratosphere, but the E3SM simulated patterns show large biases at altitudes above 50 hPa in the stratosphere (Figs. 4 and 5). The Pacific (Atlantic) sector of AO and NAO in the Z500 anomalies is much stronger (weaker) in E3SM than in observations (Fig. 10d, h). These biases of AO and NAO patterns are expected to influence the related low-level

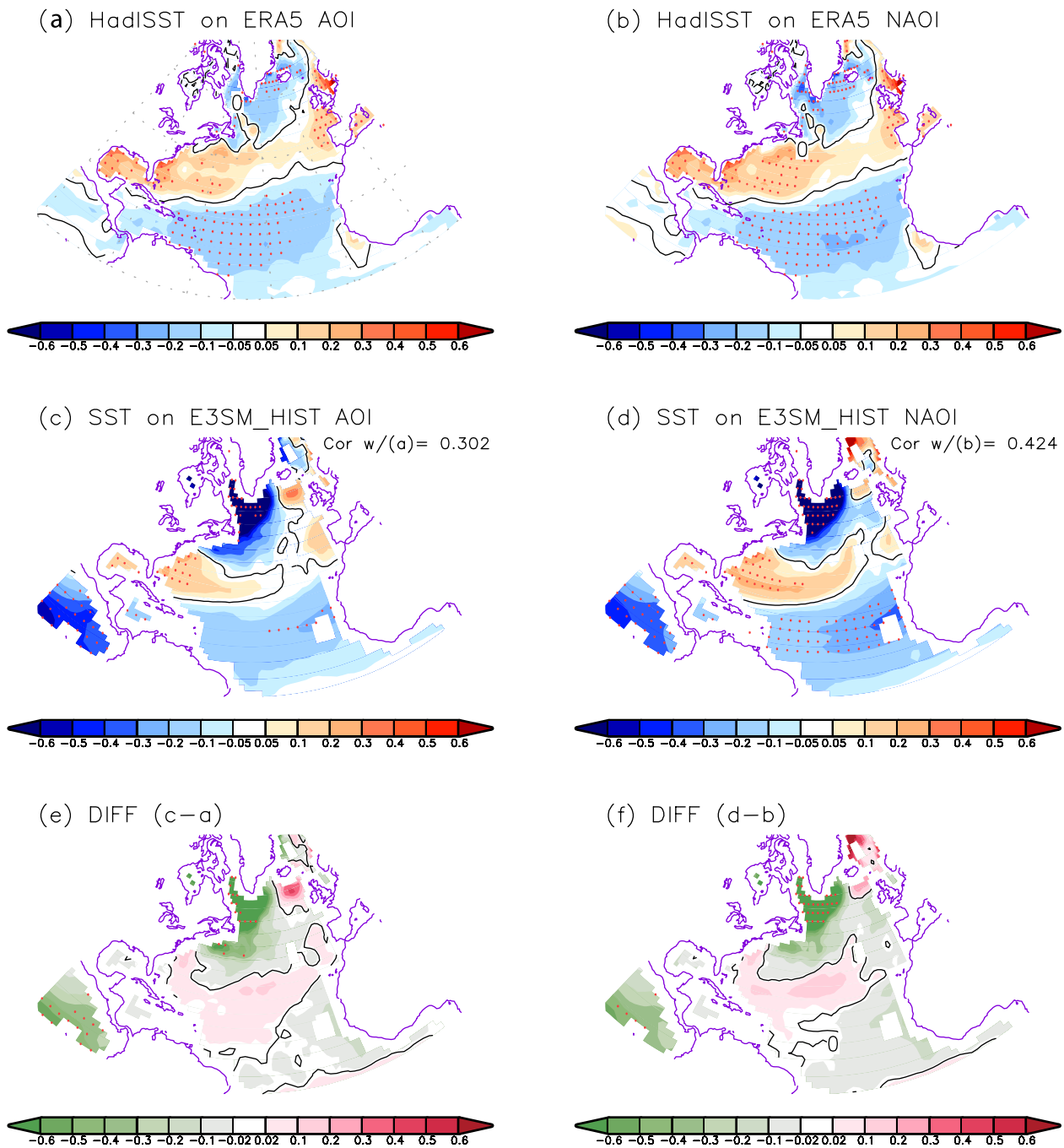

Fig. 8 Wintertime (JFM) (**a**, **b**) observed (HadISST) and **c**, **d** simulated (E3SM-HIST) sea surface temperature (SST, unit: K) anomaly patterns regressed on the JFM **a**, **c** AO and **b**, **d** NAO indices of **a**, **b** ERA5 and **c**, **d** E3SM-HIST dataset in the North Atlantic Ocean (100°W–10°E, 0°–85°N) for the period 1979-2014. **e**–**f** The differences of regressed SST patterns between E3SM-HIST and ERA5. Red stippled area indicates statistical significance at the 95% confidence level for a two-tailed Student's *t* test

temperature (T2m) anomalies (in Fig. 7d, h). Similar to other variables, the NAO-related Z500 anomalies generally show considerably weaker biases compared to AO-related Z500 anomalies.

The regressed upper level (300 hPa) zonal wind anomaly patterns onto the JFM AO and NAO indices from E3SM-HIST simulation are generally consistent with those from two reanalyses (Fig. 11). Their PCCs are about 0.58 for

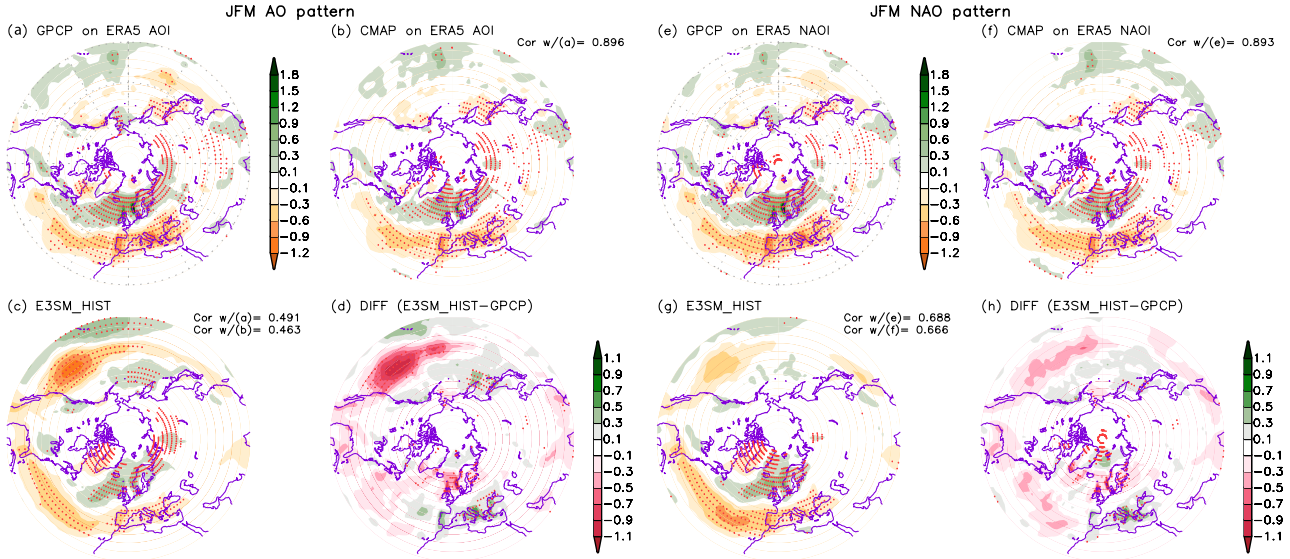

Fig. 9 Wintertime (JFM) precipitation (unit: mm/day) anomaly patterns from **a**, **e** GPCP and **b**, **f** CMAP data regressed on the JFM **a**–**c** AO and **e**–**g** NAO indices over the Northern Hemisphere (20°N–90°N) in ERA5 and E3SM-HIST dataset for the period 1979–2014. **d**, **h** The differences of regressed precipitation patterns between E3SM-HIST and GPCP. Red stippled area indicates statistical significance at the 95% confidence level for a two-tailed Student's *t* test

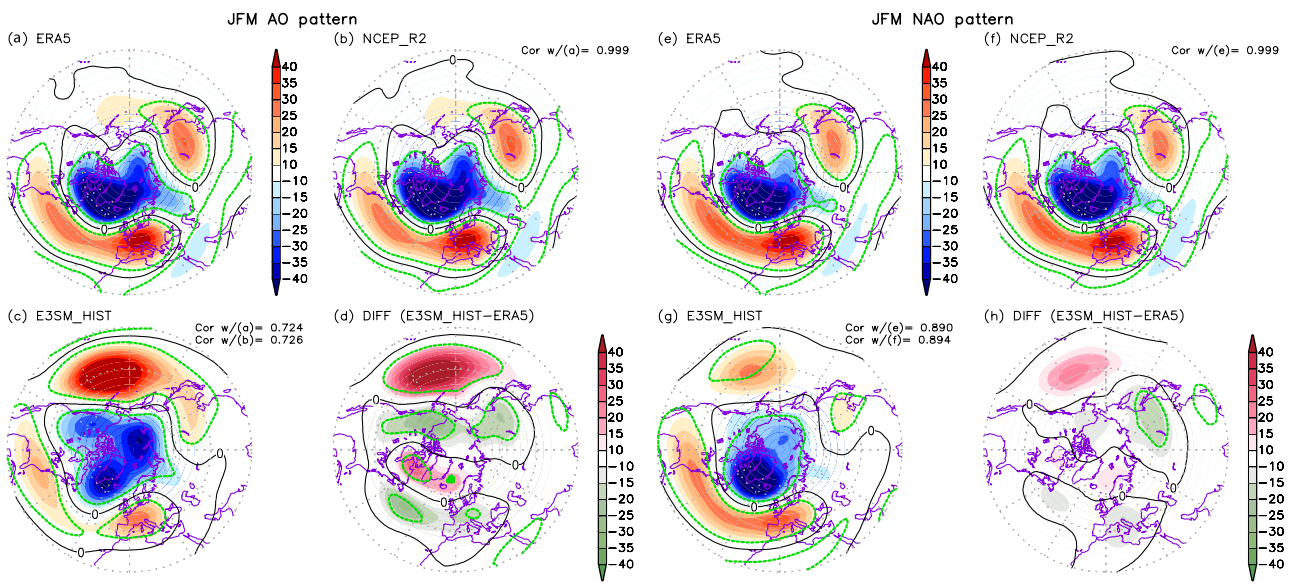

Fig. 10 Wintertime (JFM) 500 hPa geopotential height (Z500, unit: m) anomaly patterns regressed on the JFM **a**–**c** AO and **e**–**g** NAO indices over the Northern Hemisphere (20°N–90°N) in **a**, **e** ERA5, **b**, **f** NCEP-R2, and **c**, **g** E3SM-HIST dataset for the period 1979–2014. **d**, **h** The difference of regressed Z500 anomaly patterns between E3SM-HIST and ERA5. Green dashed line indicates statistical significance at the 95% confidence level for a two-tailed Student's *t* test

AO mode and about 0.83 for NAO mode. But there are systematic biases such as amplitudes at the centers of wind variability and shifts in the location of maximum variability (Fig. 11d, h). These biases correspond to those in the variability of other variables, especially over the North Atlantic and North Pacific sectors (see also Kang et al. 2014; Gong et al. 2017). NAO-associated 300 hPa zonal wind shows much stronger wind (westerly and easterly) dipole bands in the north–south direction over the Euro-North Atlantic sector than AO-associated 300 hPa zonal

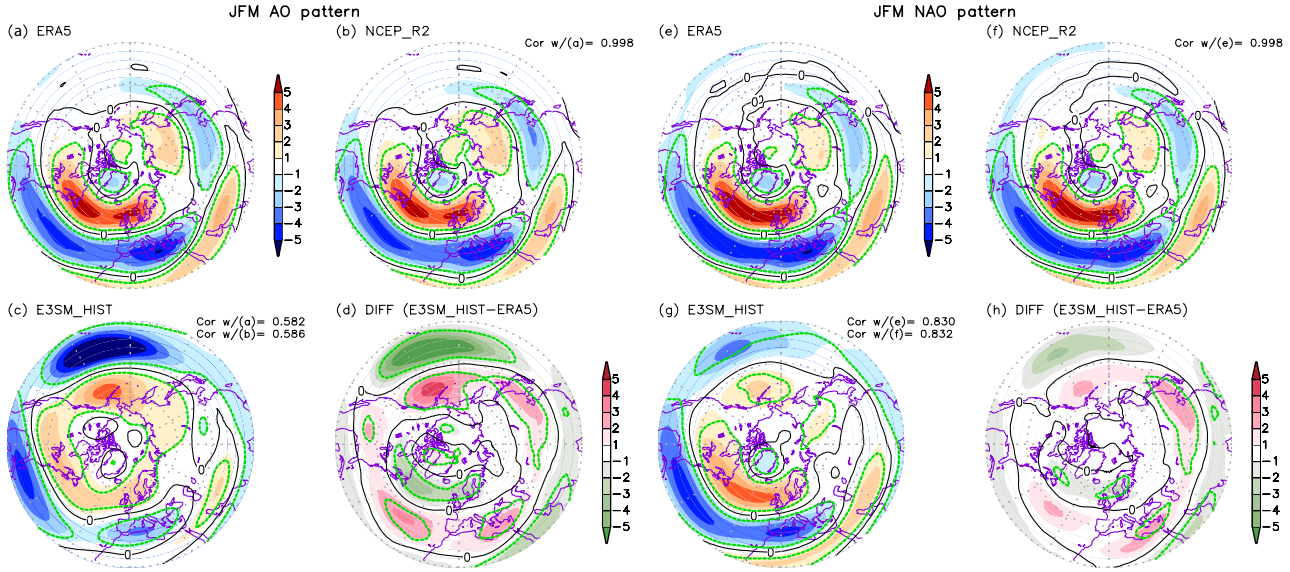

Fig. 11 Same as Fig. 10, except for 300 hPa zonal wind (U300, unit: m/s) anomaly

wind in both the simulation and observations. Due to the weaker westerly(easterly) air flow associated with wintertime AO and NAO modes over the Euro-North Atlantic (Greenland and northern Canada) in E3SM-HIST simulation compared to the observed wind patterns, cold (warm) bias are produced over northern Europe (Greenland/northeastern Canada) (see Fig. 7d, h). Figure 12 shows the winter AO and NAO-associated zonal wind patterns in the lower stratosphere (20 hPa). Observed stratospheric zonal winds are mostly zonally symmetric between the polar cap region and the mid-latitudes, and both the AO and NAO wind patterns show considerable similarity, although there is some difference in the amplitude of easterlies over North America. These features such as annular structure can be expected from the vertical structure of zonal mean zonal wind in Fig. 4 in advance. Unlike the tropospheric zonal wind patterns associated with JFM AO and NAO modes in Fig. 11, the E3SM-HIST appears to have difficulty to capture the

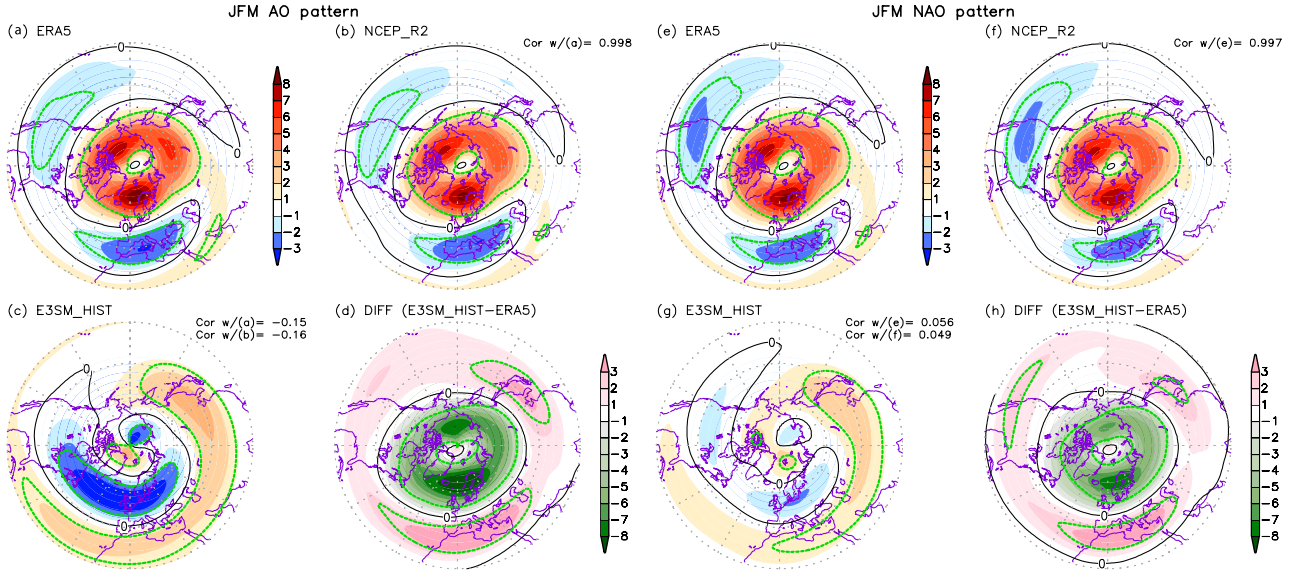

Fig. 12 Same as Fig. 10, except for 20 hPa zonal wind (U20, unit: m/s) anomaly

observed distinct features in both the AO and NAO-associated stratospheric zonal wind patterns. The performance of stratospheric zonal wind with respect to the AO and NAO modes in E3SM-HIST simulation shows the clear need for improvement.

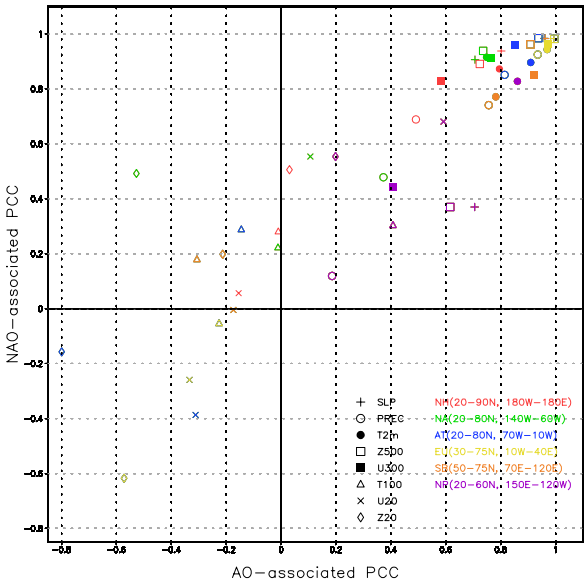

Fig. 13 Scatter diagram on wintertime (JFM) AO and NAO-associated pattern correlation coefficients for 6 regions from regression fields of 8 variables on JFM AO and NAO indices in E3SM-HIST and observations (ERA5 and GPCP). Regions: Northern Hemisphere (NH: 20–90° N, 180° W–180° E), North America (NA: 20–80° N, 140–60° W), Atlantic (AT: 20–80° N, 70–10° W), Europe (EU: 30–75° N, 10° W–40° E), Siberia (SB: 50–75° N, 70–120° E), North Pacific (NP: 20–60° N, 150° E–120° W). Variables: SLP, PREC, T2m, Z500, U300, T100, U20, and Z20

To simply understand the performance in the response patterns of various variables influenced by wintertime AO and NAO modes in E3SM-HIST simulation, the relationship between winter AO and NAO-related spatial pattern correlation coefficients is shown as the scatter diagram in Fig. 13. After obtaining the regression patterns of 8 variables onto winter AO and NAO modes in both the simulation and observations, the pattern correlation coefficients for 6 regions are calculated, and then the scatter diagram is depicted. Skills for atmospheric variables in troposphere (SLP, PREC, T2m, Z500, and U300) mostly display better performance than those in stratosphere (T100, U20, and Z20) in the AO and NAO modes. This result is consistent with the performance of AO and NAO-associated vertical structures from E3SM-HIST simulation in Figs. 4 and 5. As compared to other regions, most of tropospheric variables, except for T2m, in the North Pacific region have much lower skills due to the biases in the exaggerated Pacific center associated with winter AO and NAO exist in almost all simulated tropospheric variables. In general, the regional PCC values of AO and NAO-related variables are largely aligned along the diagonal line which are directly proportional to each other.

Figure 14 illustrates the temporal evolution of regionally averaged geopotential height (Z), zonal wind (U), and temperature (T) anomalies associated with wintertime AO and NAO indices to examine the impact and propagation of the AO and NAO signals between stratosphere and troposphere. In ERA5 and NCEP-R2, pronounced downward propagation

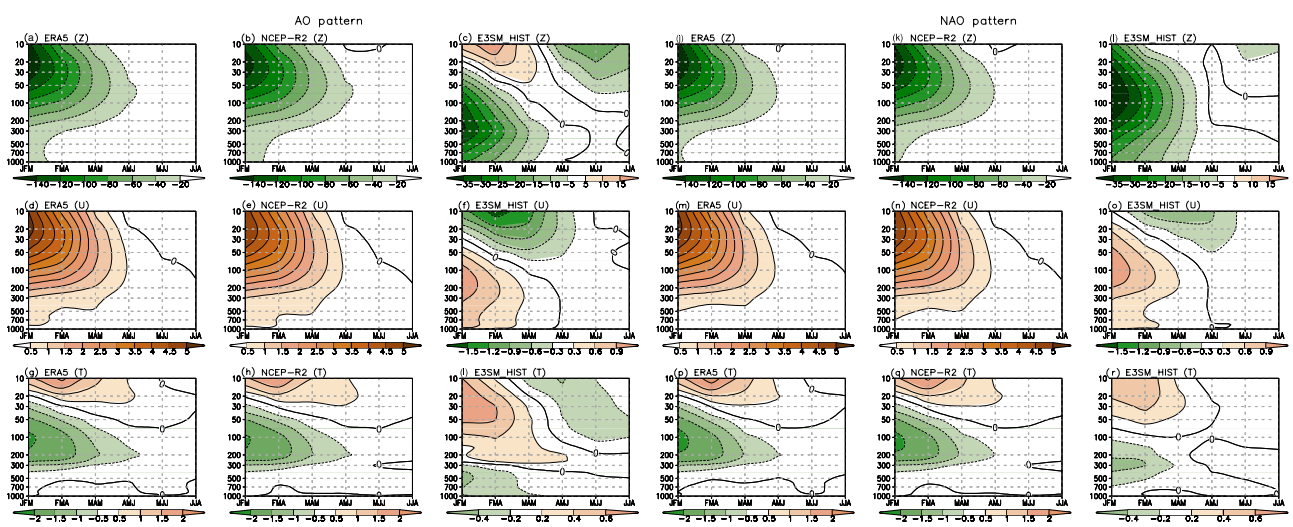

Fig. 14 Time-height evolution of 3-month averaged zonal mean anomaly patterns for (top) geopotential height (Z, unit: m), (middle) zonal wind (U, unit: m/s), and (bottom) temperature (T, unit: K) in the 1000-10 hPa layer regressed on the wintertime (JFM) **a–i** AO and **j–r** NAO indices in ERA5, NCEP-R2, and E3SM-HIST for the period 1979–2014. Z and T are zonally averaged between 70° N and 90° N, and U is zonally averaged between 60° N and 80° N

of the winter AO and NAO-related zonal mean anomalies (Z, U, and T) in the stratosphere is shown to enter the troposphere with an oscillation period of several months. These features are also present in the vertical patterns of zonal mean anomalies of various variables associated with stratospheric polar vortex (SPV) signal in previous studies (Baldwin and Dunkerton 2001; Wanner et al. 2001; Zuo et al. 2016). These studies found that wintertime SPV index shows similar characteristic to winter AO and NAO modes. When the JFM AO and NAO indices are in the positive (negative) phase, negative (positive) Z and westerly (easterly) U anomalies propagate from the stratosphere to the troposphere. In the case of temperature, stratospheric warming and cooling signals associated with observed AO and NAO modes during winter show downward extension that weakens with time. Observed propagation patterns of the JFM AO signal are almost identical to those of JFM NAO signal. In E3SM-HIST simulation, even though the center locations of the impact with respect to the phase of AO and NAO indices do not match well with those in observations, the characteristic of downward propagating with time lag appears similar to the observations. In addition, the amplitude of the zonal mean anomaly patterns in E3SM-HIST appears to be weaker than that in observations. Downward propagation patterns of zonal mean anomalies associated with NAO mode in E3SM look more like those in observations compared to the AO mode in E3SM.

7 Relationship between stratospheric polar vortex strength and stratospheric bias

Gong et al. (2019a) indicated that the strength of the climatological stratospheric polar vortex (SPV, Castanheira and Graf 2003), as represented by the 50-hPa zonal-mean zonal winds along 65° N, is tightly related to upward and eastward wave activity flux over the North Pacific and downward planetary wave activity flux over the North Atlantic and northern North America in the upper troposphere and lower stratosphere. Based on this relationship, we have investigated the possible mechanism of the climatological SPV influence on the stratospheric biases related to the AO and NAO modes in the E3SM model. To fairly compare to Gong et al. (2019a), the SPV from the zonal-mean zonal winds (Fig. 15a–c) and the horizontal and vertical component of the wave activity fluxes (Fig. 15d–f) for climatological December–January–February (DJF) season are examined. Although E3SM-HIST simulation shows strong zonal-mean zonal winds in the upper stratosphere (near 10 hPa), the climatological SPV in observations (18.89 m/s for ERA5 and 19.02 m/s for NCEP-R2) is much stronger than that in E3SM-HIST simulation (17.25 m/s). Under the criterion (18 m/s) used by Sun and Tan (2013) and Gong et al. (2019a) for classifying the strong and weak climatological SPV, both ERA5 and NCEP-R2 reanalyses would belong in the strong SPV group, similar to Japanese 55-year Reanalysis (JRA-55) in Fig. 4 of Gong et al. (2019a), while the E3SM-HIST simulation belongs in the weak SPV group. In observations, the strong climatological SPV suggests that there are strong eastward propagating wave fluxes from East Asia to the North Atlantic as well as the strong upward (downward) wave activity flux over the North Pacific (North Atlantic and northern North America) in the upper troposphere and lower stratosphere. These wave flux activities influence the active coupling of troposphere and stratosphere through changing the vertical propagation of planetary waves. In the E3SM-HIST simulation, the vertical wave activity fluxes are much weaker in companion with the weak climatological SPV compared to the observation (Fig. 15d–f), suggesting a weaker coupling between the troposphere and the stratosphere. The climatological distribution of the wave activity fluxes for the JFM season (not shown) of this study also shows similar results in the DJF season. In short, the tropospheric planetary waves may be trapped in the troposphere by the lack of activity of vertical wave fluxes under the weak climatological SPV. The resulting weaker coupling between troposphere and stratosphere likely plays a role on the less coherent vertical structure associated with AO and NAO from upper troposphere to lower stratosphere compared to the observations, as seen in Fig. 4. In fact, we find that the CMIP5 models that have large stratospheric biases in the AO index-regressed DJF zonal-mean zonal wind as in Fig. 4 of Zuo et al. (2013b) match well with the CMIP5 models that have weak climatological SPV as in Fig. 4 of Gong et al. (2019a). In addition, Gong et al. (2019a) mentioned that increasing the vertical resolution of climate models may weaken the climatological SPV and reduce the bias in the amplitude of the AO-related North Pacific center. However, although E3SM-HIST simulation with 72 levels, which would belong in the higher vertical-resolution group among the CMIP5 models in Gong et al. (2019a), has weak climatological SPV, the fact that the amplitude of the North Pacific center in the AO and NAO pattern is still stronger than observations needs to be further examined as well as the stratospheric biases associated with AO and NAO modes.

8 Summary and conclusion

As part of the critical evaluation of the overall performance of E3SM, this study assesses the ability of the model to simulate the AO and NAO, which are known to be important modes of wintertime climate variability in the Northern Hemisphere. The model data used in this diagnostic study consist of the historical simulations with 5 ensemble members for the 36-year period of 1979–2014 performed with

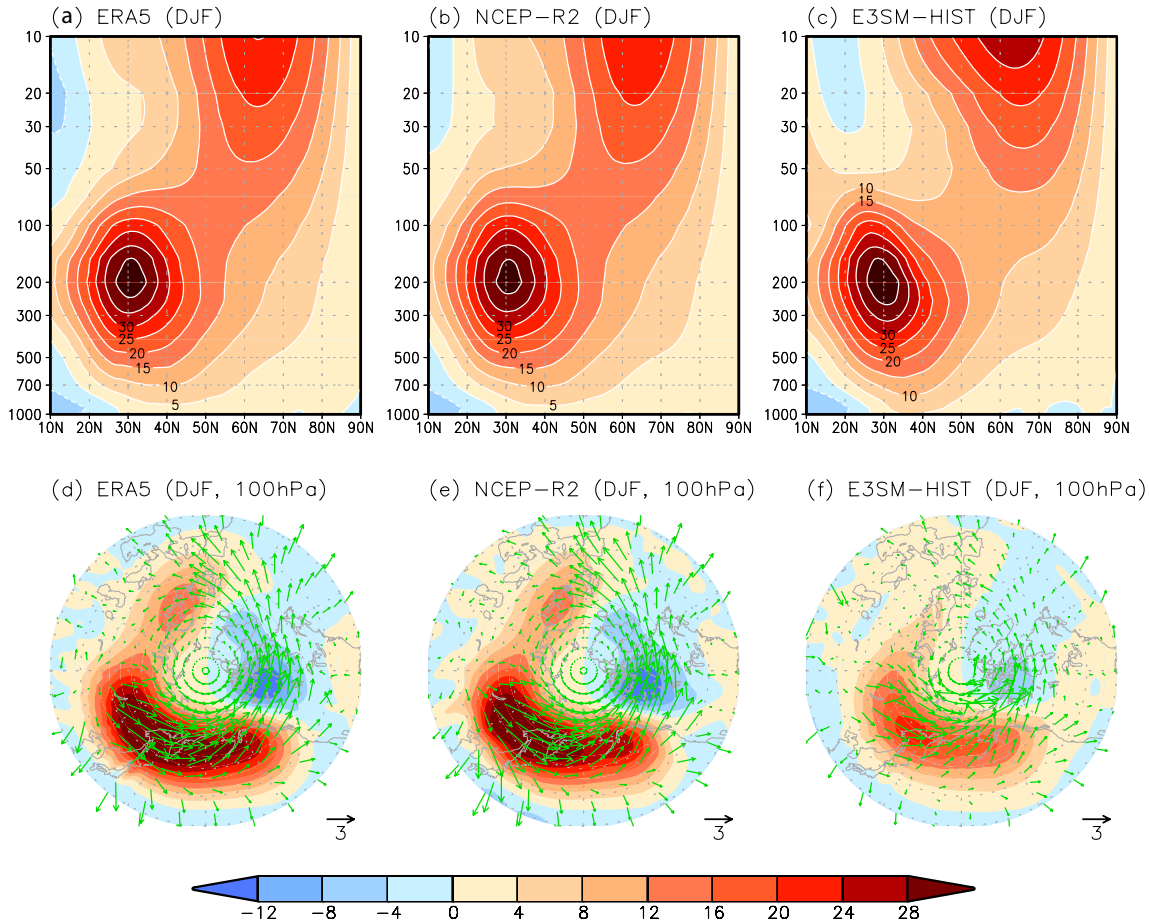

Fig. 15 (Top) Vertical structures of the climatological wintertime (December-February: DJF) zonal-mean zonal wind (unit: m/s) in ERA5, NCEP-R2, and E3SM-HIST for the period 1979–2013. Contour intervals are 5 m/s. Climatological distribution of the (bottom) DJF planetary wave activity fluxes at 100 hPa. The arrows and shading indicate the horizontal (unit: m^2/s^2) and vertical (unit: 10^{-3} m^2/s^2) component of wave activity flux, respectively. The positive (negative) vertical component means the upward (downward) motion

the Energy Exascale Earth System Model (E3SM-HIST). We analyze the performance and characteristics of the wintertime AO and NAO variability, and their impacts over the Northern Hemisphere in E3SM-HIST simulations.

We first examine the observed vertical structure of zonal mean Z, U, and T anomalies for ERA5 and NCEP-R2, associated with the monthly AO and NAO indices. After calculating the magnitude of annual variation by using the vertical location of the largest variability related to AO and NAO modes, we selected the months January to March (JFM) to represent the AO and NAO-associated active season.

Regressed horizontal/vertical structures as typical patterns associated with the positive phase of wintertime AO and NAO in E3SM are compared with observations. We find that the E3SM-HIST exhibits a quasi-barotropic structure and meridional dipole pattern that are consistent with observed features, but still has difficulties in simulating the magnitude of the activity center of the horizontal structure that were also reported in previous works (e.g., Miller et al. 2006; Cattiaux and Cassou 2013; Gong et al. 2017). The model also has considerable biases in both amplitude and center location of vertical patterns in the lower stratosphere (see also Zuo et al. 2013b).

In the power spectral analysis for the time series of the wintertime AO and NAO indices, generally, it turns out that the observed AO and NAO spectrum patterns consist of similar leading signals with near-identical quasi-periodicity. E3SM-HIST simulations capture well the nearly 3.5-year cycle in the AO-related time variability and nearly 2.4 and 5–5.5-year cycle in the NAO-related time variability, even though showing a reversed power spectrum pattern as a function of period compared to observations.

The climate impacts on several variables with regard to wintertime AO and NAO modes are further investigated. Like the previous findings (Deser 2000; Ambaum et al. 2001; Wallace and Thompson 2002) that it is not easy to differentiate the relative climate impacts between AO and NAO modes, the dominant features of climate variability

associated with JFM AO and NAO modes in both the simulation and observations are similar to each other. Overall, the AO and NAO-associated spatial impacts and main structural features in the E3SM-HIST simulation are analogous to those in observations. However, systematic biases in simulations such as amplitudes in the centers and shifts in the maximum location in terms of AO and NAO-related variability, especially over the North Atlantic and North Pacific sectors, need improvement. From comparing the performance of climate impacts associated with the simulated winter AO and NAO modes, we find that the skills in capturing the association with tropospheric variables generally are much higher than those of stratospheric variables due to deficiencies in the stratospheric simulation of E3SM-HIST. Performance of simulating the AO versus NAO-related variability among variables seem to be almost proportional to one another, but the climate impacts associated with NAO have a tendency to be better simulated.

To examine the downward influence of stratospheric variability with time, time-height evolution of each vertical variable related to wintertime AO and NAO modes is shown. Downward propagating signals from the lower stratosphere with a period of several months in observation are found. We also find the downward propagating pattern similar to observations with time lag in the E3SM-HIST simulation, although the center location and amplitude of winter AO and NAO-related vertical impacts in E3SM-HIST do not match well with those in observations.

Based on the results that show close relationship between the intensity of climatological SPV and the horizontal/vertical wave activity flux in Gong et al. (2019a), we explore the possible causes of occurrence of the stratospheric biases related to the AO and NAO modes in the E3SM-HIST simulations. In the E3SM-HIST simulation with a weaker climatological SPV compared to the observations, it is found that weaker horizontal/vertical wave flux activities may affect the vertical coupling between the troposphere and stratosphere. We postulate that the weaker vertical coupling due to the lack of wave activity flux results in the large stratospheric biases in the vertical structures associated with AO and NAO in E3SM.

We have demonstrated that E3SM-HIST has a capability to reproduce the observed characteristics in the JFM AO and NAO-associated vertical/horizontal spatial patterns. It is also noteworthy that the climate impacts with regard to JFM AO and NAO modes match reasonably well with observations. However, there is still room for improvement in the amplitude and location of the winter AO and NAO-associated spatial pattern and variability as the same biases have been reported in most other climate models. In addition, though the topic of the causes of the systematic biases on climate impacts of stratospheric variability associated with AO and NAO was briefly covered by the relationship between climatological SPV and stratospheric bias in this study, it should remain an area of interest that needs to be studied for the improvement of current climate predictability and future climate projections made by E3SM simulations.

Acknowledgements This research was supported as part of the Energy Exascale Earth System Model (E3SM) project, funded by the U.S. Department of Energy, Office of Science, Office of Biological and Environmental Research. NCEP Reanalysis 2, GPCP Precipitation, and CMAP Precipitation data are provided by the NOAA/OAR/ESRL PSD, Boulder, Colorado, USA, from their Web site at https://www.esrl.noaa.gov/psd/. ERA5 reanalysis data are available from https://cds.climate.copernicus.eu/cdsapp#!/home. HadISST SST data are available from https://www.metoffice.gov.uk/hadobs/hadisst/. E3SM data are freely available through the Earth System Grid Federation (ESGF) distributed archives. See details at https://e3sm.org/data. E3SM simulations are conducted at Argonne Leadership Computing Facility (contract DE-AC02-06CH11357); National Energy Research Scientific Computing Center (DE-AC02-05CH11231); Oak Ridge Leadership Computing Facility (DE-AC05-00OR22725); Argonne National Laboratory high-performance computing cluster, provided by BER Earth System Modeling; and Los Alamos National Laboratory Institutional Computing, U.S. DOE NNSA (DE-AC02-05CH11231).

References

Adler RF et al (2003) The version-2 global precipitation climatology project (GPCP) monthly precipitation analysis (1979–Present). J Hydrometeorol 4:1147–1167

Ambaum MHP, Hoskins BJ, Stephenson DB (2001) Arctic Oscillation or North Atlantic Oscillation? J Clim 14:3495–3507

Arakawa A, Lamb VR (1977) Computational design of the basic dynamical processes of the UCLA general circulation model. Methods in computational physics: advances in research and applications. In: Chang J (ed) General circulation models of the atmosphere, vol 17. Elsevier, Amsterdam, pp 173–265. https://doi.org/10.1016/B978-0-12-460817-7.50009-4

Baldwin MP, Dunkerton TJ (2001) Stratospheric Harbingers of Anomalous Weather Regimes. Science 294(5542):581–584. https://doi.org/10.1126/science.1063315

Castanheira JM, Graf HF (2003) North Pacific-North Atlantic relationships under stratospheric control? J Geophys Res Atmos. https://doi.org/10.1029/2002jd002754

Cattiaux J, Cassou C (2013) Opposite CMIP3/CMIP5 trends in the wintertime Northern Annular Mode explained by combined local sea ice and remote tropical influences. Geophys Res Lett 40:3682–3687. https://doi.org/10.1002/grl.50643

Chen S, Chen W, Yu B, Graf HF (2013) Modulation of the seasonal footprinting mechanism by the boreal spring Arctic Oscillation. Geophys Res Lett 40:6384–6389. https://doi.org/10.1002/2013GL058628

Cohen J, Barlow M (2005) The NAO, the AO, and global warming: how closely related? J Clim 18(21):4498–4513. https://doi.org/10.1175/JCLI3530.1

Czaja A, Frankignoul C (2002) Observed Impact of Atlantic SST Anomalies on the North Atlantic Oscillation. J Clim 15:606–623. https://doi.org/10.1175/1520-0442(2002)015%3c0606:OIOASA%3e2.0.CO;2

Davini P, Cagnazzo C (2014) On the misinterpretation of the North Atlantic Oscillation in CMIP5 models. Clim Dyn 43:1497–1511. https://doi.org/10.1007/s00382-013-1970-y

Deser C (2000) On the teleconnectivity of the "Arctic Oscillation". Geophys Res Lett 27(6):779–782. https://doi.org/10.1029/1999GL010945

Driscoll S, Bozzo A, Gray LJ, Robock A, Stenchikov G (2012) Coupled Model Inter-comparison Project 5 (CMIP5) simulations of climate following volcanic eruptions. J Geophys Res Atmos. https://doi.org/10.1029/2012jd017607

Eyring V, Bony S, Meehl GA, Senior CA, Stevens B, Stouffer RJ, Taylor KE (2016) Overview of the Coupled Model Intercomparison Project Phase 6 (CMIP6) experimental design and organization. Geosci Model Dev 9:1937–1958. https://doi.org/10.5194/gmd-9-1937-2016

Feldstein SB, Franzke C (2006) Are the North Atlantic oscillation and the northern annular mode distinguishable? J Atmos Sci 63:2915–2930. https://doi.org/10.1175/JAS3798.1

Golaz JC et al (2019) The DOE E3sm Coupled Model Version 1: overview and Evaluation at Standard Resolution. J Adv Model Earth Syst 11:2089–2129. https://doi.org/10.1029/2018MS001603

Gong DY, Wang SW, Zhu JH (2001) East Asian winter monsoon and arctic oscillation. Geophys Res Lett 28(10):2073–2076. https://doi.org/10.1029/2000GL012311

Gong H, Wang L, Chen W, Wu R, Wei K, Cui X (2014) The climatology and interannual variability of the East Asian winter monsoon in CMIP5 models. J Clim 27:1659–1678

Gong H, Wang L, Chen W, Nath D, Huang G, Tao W (2015) Diverse influences of ENSO on the East Asian–western Pacific winter climate tied to different ENSO properties in CMIP5 models. J Clim 28:2187–2202

Gong H, Wang L, Chen W, Chen X, Nath D (2017) Biases of the wintertime Arctic Oscillation in CMIP5 models. Environ Res Lett 12(014):001. https://doi.org/10.1088/1748-9326/12/1/014001

Gong H, Wang L, Chen W, Nath D (2018) Multidecadal fluctuation of the wintertime Arctic Oscillation pattern and its implication. J Clim 31:5595–5608

Gong H, Wang L, Chen W, Wu R, Zhou W, Liu L, Nath D, Lan X (2019a) Diversity of the wintertime Arctic oscillation pattern among cmip5 Models: role of the stratospheric polar vortex. J Clim 32:5235–5250

Gong H, Wang L, Chen W (2019b) Multidecadal changes in the influence of the Arctic oscillation on the East Asian Surface air temperature in boreal winter. Atmosphere 10:757. https://doi.org/10.3390/atmos10120757

Greatbatch RJ (2000) The North Atlantic Oscillation. Stoch Environ Res Risk Assess 14(4):213–242. https://doi.org/10.1007/s004770000047

He S, Gao Y, Li F, Wang H, He Y (2017) Impact of Arctic Oscillation on the East Asian climate: a review. Earth Sci Rev 164:48–62. https://doi.org/10.1016/j.earscirev.2016.10.014

Hersbach H et al (2018) Operational global reanalysis: progress, future directions and synergies with NWP. ERA Rep Seri 27:1–63. https://doi.org/10.21957/tkic6g3wm

Hunke EC, Dukowicz JK (1997) An elastic–viscous–plastic model for sea ice dynamics. J Phys Oceanogr 27:1849–1867. https://doi.org/10.1175/1520-0485(1997)027%3c1849:AEVPMF%3e2.0.CO;2

Hurrell JW (1995) Decadal Trends in the North Atlantic Oscillation: regional Temperatures and Precipitation. Science 269(5224):676–679. https://doi.org/10.1126/science.269.5224.676

Hurrell JW (1996) Influence of variations in extratropical wintertime teleconnections on northern hemisphere temperature. Geophys Res Lett 23:665–668. https://doi.org/10.1029/96GL00459

Hurrell JW, Deser C (2010) North Atlantic climate variability: the role of the North Atlantic Oscillation. J Mar Syst 79:231–244. https://doi.org/10.1016/j.jmarsys.2009.11.002

Hurrell JW, Deser C (2015) Northern Hemisphere climate variability during winter: looking back on the work of Felix Exner. Meteorol Z 24:113–118. https://doi.org/10.1127/metz/2015/0578

Hurrell JW, van Loon H (1997) Decadal variations in climate associated with the North Atlantic Oscillation. Clim Change 36:301–326. https://doi.org/10.1023/A:1005314315270

Hurrell JW, Kushnir Y, Ottersen G, Visbeck M (2003) An Overview of the North Atlantic Oscillation. N Atl Oscil Clim Sig Environ Impact Am Geophys Union (AGU). https://doi.org/10.1029/134gm01

Jevrejeva S, Moore JC, Grinsted A (2003) Influence of the Arctic Oscillation and El Ni no-Southern Oscillation (ENSO) on ice conditions in the Baltic Sea: the wavelet approach. J Geophys Res Atmos. https://doi.org/10.1029/2003jd003417

Jevrejeva S, Moore JC, Woodworth PL, Grinsted A (2005) Influence of large-scale atmospheric circulation on European sea level: results based on the wavelet transform method. Tellus A 57(2):183–193. https://doi.org/10.1111/j.1600-0870.2005.00090.x

Kanamitsu M, Ebisuzaki W, Woollen J, Yang SK, Hnilo JJ, Fiorino M, Potter GL (2002) NCEP–DOE AMIP-II Reanalysis (R-2). Bull Am Meteorol Soc 83(11):1631–1644. https://doi.org/10.1175/BAMS-83-11-1631

Kang D et al (2014) Prediction of the Arctic Oscillation in boreal winter by dynamical seasonal forecasting systems. Geophys Res Lett 41(10):3577–3585. https://doi.org/10.1002/2014GL060011

Kushnir Y (1999) Europe's winter prospects. Nature 398(6725):289–291. https://doi.org/10.1038/18560

Kushnir Y, Wallace JM (1989) Low-frequency variability in the northern hemisphere winter: geographical distribution, structure and time-scale dependence. J Atmos Sci 46(20):3122–3143. https://doi.org/10.1175/1520-0469(1989)046%3c3122:LFVITN%3e2.0.CO;2

Li H, Wigmosta MS, Wu H, Huang M, Ke Y, Coleman AM, Leung LR (2013) A physically based runoff routing model for land surface and earth system models. J Hydrometeorol 14(3):808–828. https://doi.org/10.1175/JHM-D-12-015.1

Li HY, Leung LR, Getirana A, Huang M, Wu H, Xu Y, Guo J, Voisin N (2015) Evaluating global streamflow simulations by a physically based routing model coupled with the community land model. J Hydrometeorol 16(2):948–971. https://doi.org/10.1175/JHM-D-14-0079.1

Marshall J et al (2001) North Atlantic climate variability: phenomena, impacts and mechanisms. Int J Climatol 21(15):1863–1898. https://doi.org/10.1002/joc.693

Miller RL, Schmidt GA, Shindell DT (2006) Forced annular variations in the 20th century Intergovernmental Panel on Climate Change Fourth Assessment Report models. J Geophys Res Atmos. https://doi.org/10.1029/2005jd006323

Oleson K et al (2013) Technical description of version 4.5 of the Community Land Model (CLM). (Tech. Rep. NCAR/TN-503 + STR), https://doi.org/10.5065/d6rr1w7m

Petersen MR, Jacobsen DW, Ringler TD, Hecht MW, Maltrud ME (2015) Evaluation of the arbitrary Lagrangian-Eulerian vertical coordinate method in the MPAS-Ocean model. Ocean Model 86:93–113

Petersen MR et al (2019) an evaluation of the ocean and sea ice climate of E3smUsing MPAS and interannual CORE-II forcing. J Adv Model Earth Syst 11(5):1438–1458. https://doi.org/10.1029/2018MS001373

Rasch PJ et al (2019) An overview of the atmospheric component of the energy exascale earth system model. J Adv Model Earth Syst 11(8):2377–2411. https://doi.org/10.1029/2019MS001629

Rayner NA, Parker DE, Horton EB, Folland CK, Alexander LV, Rowell DP, Kent EC, Kaplan A (2003) Global analyses of sea surface temperature, sea ice, and night marine air temperature since

the late nineteenth century. J Geophys Res Atmos. https://doi.org/10.1029/2002jd002670

Ringler TD, Thuburn J, Klemp JB, Skamarock WC (2010) A unified approach to energy conservation and potential vorticity dynamics for arbitrarily-structured C-grids. J Comput Phys 229(9):3065–3090. https://doi.org/10.1016/j.jcp.2009.12.007

Rogers J, McHugh M (2002) On the separability of the North Atlantic oscillation and Arctic oscillation. Clim Dyn 19(7):599–608. https://doi.org/10.1007/s00382-002-0247-7

Stoner AMK, Hayhoe K, Wuebbles DJ (2009) Assessing general circulation model simulations of atmospheric teleconnection patterns. J Clim 22(16):4348–4372. https://doi.org/10.1175/2009JCLI2577.1

Sun J, Tan B (2013) Mechanism of the wintertime Aleutian low–Icelandic low seesaw. Geophys Res Lett 40:4103–4108. https://doi.org/10.1002/grl.50770

Tang Q et al (2019) Regionally refined test bed in E3SM atmosphere model version1 (EAMv1) and applications for high-resolution modeling. Geosci Model Dev 12(7):2679–2706. https://doi.org/10.5194/gmd-12-2679-2019

Thompson DWJ, Wallace JM (1998) The Arctic oscillation signature in the wintertime geopotential height and temperature fields. Geophys Res Lett 25(9):1297–1300. https://doi.org/10.1029/98GL00950

Thompson DWJ, Wallace JM (2000) Annular modes in the extratropical circulation. Part I: month-to-month variability. J Clim 13(5):1000–1016. https://doi.org/10.1175/1520-0442(2000)013%3c1000:amitec%3e2.0.co;2

Thompson DWJ, Wallace JM (2001) Regional climate impacts of the Northern Hemisphere annular mode. Science 293:85–89. https://doi.org/10.1126/science.1058958

van Loon H, Rogers JC (1978) The seesaw in winter temperatures between Greenland and Northern Europe. Part I: general Description. Mon Weather Rev 106:296–310. https://doi.org/10.1175/1520-0493(1978)106%3c0296:TSIWTB%3e2.0.CO;2

Wallace JM (2000) North Atlantic Oscillation/annular mode: two paradigms-one phenomenon. Q J R Meteorol Soc 126:791–805. https://doi.org/10.1002/qj.49712656402

Wallace JM, Gutzler DS (1981) Teleconnections in the geopotential height field during the Northern hemisphere winter. Mon Weather Rev 109:784–812. https://doi.org/10.1175/1520-0493(1981)109%3c0784:TITGHF%3e2.0.CO;2

Wallace JM, Thompson DWJ (2002) The Pacific center of action of the Northern Hemisphere annular mode: real or artifact? J Clim 15:1987–1991. https://doi.org/10.1175/1520-0442(2002)015%3c1987:TPCOAO%3e2.0.CO;2

Wang L, Chen W (2010) Downward Arctic Oscillation signal associated with moderate weak stratospheric polar vortex and the cold December 2009. Geophys Res Lett. https://doi.org/10.1029/2010gl042659

Wanner H, Brönnimann S, Casty C, Gyalistras D, Luterbacher J, Schmutz C, Stephenson DB, Xoplaki E (2001) North Atlantic Oscillation—concepts and studies. Surveys iGeophys 22:321–381. https://doi.org/10.1023/A:1014217317898

Wu B, Wang J (2002) Possible impacts of winter Arctic oscillation on Siberian high, the East Asian winter monsoon and sea–ice extent. Adv Atmos Sci 19:297–320. https://doi.org/10.1007/s00376-002-0024-x

Xie P, Arkin PA (1997) Global precipitation: a 17-year monthly analysis based on gauge observations, satellite estimates, and numerical model outputs. Bull Am Meteor Soc 78:2539–2558. https://doi.org/10.1175/1520-0477(1997)078%3c2539:GPAYMA%3e2.0.CO;2

Xin XG, Zhou TJ, Yu RC (2008) The Arctic oscillation in coupled climate models. Chin J Geophys 51:223–239. https://doi.org/10.1002/cjg2.1214

Zhu Y, Wang H (2010) The Arctic and Antarctic oscillations in the IPCC AR4 coupled models. J Meteorol Re 24:176–188

Zuo J, Li W, Sun C, Xu L, Ren HL (2013a) Impact of the North Atlantic sea surface temperature tripole on the East Asian summer monsoon. Adv Atmos Sci 30:1173–1186. https://doi.org/10.1007/s00376-012-2125-5

Zuo JQ, Li WJ, Ren HL (2013b) Representation of the Arctic oscillation in the CMIP5 Models. Adv Clim Change Res 4:242–249. https://doi.org/10.3724/SP.J.1248.2013.242

Zuo J, Ren HL, Wu J, Nie Y, Li Q (2016) Subseasonal variability and predictability of the Arctic oscillation/North Atlantic oscillation in BCC_agcm2.2. Dyn Atmos Oceans 75:33–45. https://doi.org/10.1016/j.dynatmoce.2016.05.002

Publisher's Note Springer Nature remains neutral with regard to jurisdictional claims in published maps and institutional affiliations.